INSTITUTE OF PHYSICS PUBLISHING WAVES IN RANDOM MEDIA

Waves Random Media **12** (2002) 175–200 PII: S0959-7174(02)27341-3

Monostatic and bistatic statistical shadowing functions from a one-dimensional stationary randomly rough surface: II. Multiple scattering

C Bourlier[1], **G Berginc**[2] **and J Saillard**[1]

[1] IRCCyN: UMR no 6597 CNRS, Division SETRA, Ecole Polytechnique de l'Université de Nantes, Batiment IRESTE, Rue Christian Pauc, La Chantrerie, BP 50609, 44306 Nantes Cedex 3, France
[2] DS/DFO, THALES Optronique, Rue Guynemer, BP 55, 78283 Guyancourt Cedex, France

E-mail: christophe.bourlier@polytech.univ-nantes.fr

Received 30 July 2001, in final form 31 October 2001
Published 18 December 2001
Online at stacks.iop.org/WRM/12/175

Abstract

The integral equation model (IEM) has been developed over the last decade and it has become one of the most widely used theoretical models for rough-surface scattering in microwave remote sensing. In the IEM model the shadowing function is typically either omitted or a form based on geometric optics with single reflection is used. In this paper, a shadowing function for one-dimensional rough surfaces which incorporates multiple scattering, finite surface length and both monostatic and bistatic configurations is developed. For any uncorrelated process, the resulting equation can be expressed in terms of the monostatic statistical shadowing function with single reflection, derived in the preceding companion paper. The effect of correlation between the surface slopes and heights for a Gaussian surface is studied to illuminate the range over which such correlations can be ignored. It is found that while the correlation between surface slopes and heights in the monostatic statistical shadowing function with single reflection can be ignored, when calculating the average shadowing function with double reflection the correlation between slopes and heights between points must be incorporated.

1. Introduction

For a very rough surface, the phenomenon of multiple scattering is important and allows us to explain the backscattering enhancement observed from experimental data [1, 2] and from computing simulation [3–6]. To predict this phenomenon, analytical models such as the integral equation model (IEM) can also be used. This method is based on the first- and second-order Kirchhoff approximation with a rough surface assumed to be stationary.

 © 2002 IOP Publishing Ltd Printed in the UK

The first version of IEM, developed by Fung [7], assumed an incorrect shape for the Weyl representation of such a Green function and its gradient. This was recognized and partially corrected in the second version, suggested by Hsieh *et al* [8–10], of the model (IEMM). However, the shape of the gradient of the Green function remained incorrect and a third version, by Chen *et al* [11], was released to amend this. Recently, Alvarez-Pérez [12] provided a consistent formulation of the IEM model denoted as IEM2M, since erroneous assumptions are made in the previous models.

In the IEM model, when the shadowing effect is not ignored, the average shadowing function with single reflection is extended to that with double reflection by a physical approach. As shown by Sancer [13] from the first-order Kirchhoff approximation, this assumption is valid with the geometric optics approximation. Bourlier *et al* [14, 15] have shown how the statistical shadowing function can be included in the bistatic scattering coefficient performed from the first-order Kirchhoff approximation.

To solve this problem, the statistical shadowing function with multiple reflection is investigated in this paper for monostatic (emitter and receiver located at the same place corresponding to the backscattering case) and bistatic (emitter and receiver locations are distinct) configurations. The statistical shadowing function with single reflection presented by Bourlier *et al* [16] for a given observation length is a starting point to determine the shadowing effect with multiple reflection. As shown in [16], for a single reflection, the statistical shadowing function carries a restriction over the surface slopes and modifies the surface height behaviour. The surface height and slope probability density function (pdf) with shadow is then obtained from the unshadowed one multiplied by the statistical shadowing function. The aim of this paper is to extend these results to a multiple-scattering problem and to discuss the consequences for the derivation of the scattering coefficient. For this analysis, the surface is assumed to be one dimensional and stationary. As shown by Bourlier *et al* [16–18], since the Smith statistical shadowing function is more accurate than Wagner's, the Smith analysis with single reflection is used for computing the statistical shadowing function with multiple reflection.

Section 2 presents the monostatic statistical shadowing function for any uncorrelated process, and applies the model for an uncorrelated Gaussian process. Section 3 extends the approach for a bistatic configuration. Since the correlation between the surface heights and slopes is ignored, the statistical shadowing function does not depend on the surface height autocorrelation function. In section 4, the correlation is investigated for a Gaussian correlated process.

2. Monostatic statistical shadowing function for any uncorrelated process

Wagner's [19] and Smith's [20,21] approaches are used to describe the shadowing function with single reflection for a stationary rough surface. Their formulation assumes that the surface is one dimensional with a Gaussian process, where the correlation between the surface slopes and heights is neglected. From these works, Bourlier *et al* [16–19] have extended the shadowing function for any uncorrelated and correlated Gaussian processes. With a Gaussian process, they showed for an infinite observation length that the Smith results are more accurate than Wagner's, and the correlation weakly improves the model. Therefore in this paper, the Smith approach is chosen as a starting point to develop the statistical shadowing function with multiple reflection.

In this section this is performed from a one-dimensional rough surface in a monostatic configuration. This function is required for the derivation of the scattering coefficient calculated from the first- and second-order Kirchhoff approximations. In section 2.1, the problem is formulated for a double reflection, and section 2.2 presents simulations. In the last section, the case of the multiple reflection is analysed.

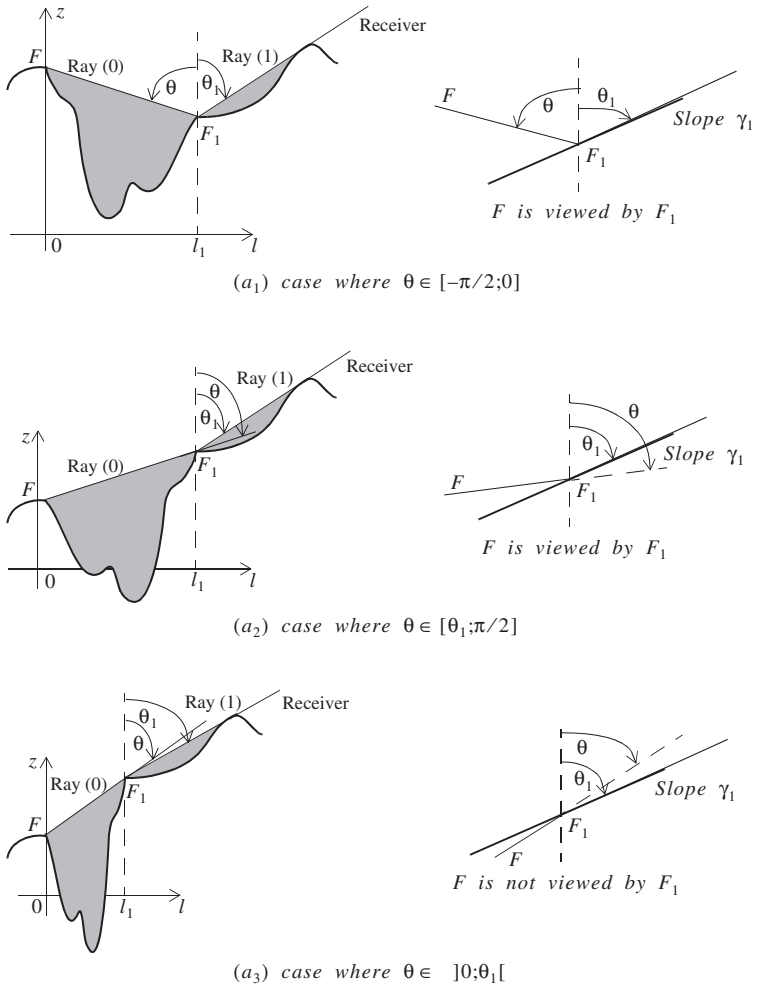

Figure 1. On the left, an illustration of the monostatic statistical shadowing function with double reflection for $\theta_1 \in [0; \pi/2]$ and $\theta \in [-\pi/2; \pi/2]$. The surface point $F(\xi_0, \gamma_0)$ is characterized by the height ξ_0 and the slope γ_0, whereas the surface point $F_1(\xi_1, \gamma_1)$ is given by $\{\xi_1 = \xi_0 + l_1 \cot\theta, \gamma_1\}$. On the right, the case where $\gamma_1 = \mu_1 = \cot\theta_1$, corresponding to the surface limit slope where the point F_1 is viewed by the receiver.

2.1. Monostatic statistical shadowing function with double reflection

As shown in figure 1, the monostatic statistical shadowing function with double reflection S_2 (subscript 2) represents the probability that the double-bounced waves denoted by the rays (0)–(1) are not intercepted by the surface. We can write that for each case (a_i) with $\theta_1 \in [0; \pi/2]$ and $\theta \in [-\pi/2; \pi/2]$

$$S_2(\mu, \mu_1, F, F_1, l_1) = \begin{cases} S(|\mu|, F, l_1) \times S(\mu_1, F_1, \infty) & \text{if} \quad \theta \in [-\pi/2; 0] \quad \text{case } (a_1) \\ S(\mu, F, l_1) \times S(\mu_1, F_1, \infty) & \text{if} \quad \theta \in [\theta_1; \pi/2] \quad \text{case } (a_2) \\ 0 & \text{if} \quad \theta \in]0; \theta_1[\quad \text{case } (a_3) \end{cases} \tag{1}$$

with $\{\mu = \cot\theta, \mu_1 = \cot\theta_1\}$ the beam slopes of the rays (0)–(1), respectively. S denotes the monostatic statistical shadowing function with single reflection and for a given observation length l_1.

For any surface height ξ_0 and slope γ_0 the uncorrelated process $p(\xi_0, \gamma_0)$ with the Smith formulation, $S(\mu, F, l_1)$, is expressed as (equations (12) and (12b) of [16])

$$S(\mu, F, l_1) = \Upsilon(\mu - \gamma_0) \times \left[\frac{P(\xi_0) - P(-\infty)}{P(\xi_0 + \mu l_1) - P(-\infty)}\right]^{\Lambda(\mu)} \qquad \begin{cases} F \equiv F(\xi_0, \gamma_0) \\ \{\mu, l_1\} \geqslant 0, \end{cases} \tag{2}$$

with

$$\Upsilon(x) = \begin{cases} 1 & \text{if} \quad x \geqslant 0 \\ 0 & \text{else,} \end{cases} \tag{2a}$$

and

$$\Lambda = \frac{1}{\mu}\int_{\mu}^{\infty} (\gamma - \mu) p(\gamma)\, \mathrm{d}\gamma \qquad P = \int p(\xi)\, \mathrm{d}\xi. \tag{2b}$$

As shown in figure 1, in the (a_3) case, we obtain $S_2 = 0$ since the point F cannot be viewed by the receiver. For cases $(a_{1,2})$, S_2 is the product of both monostatic shadowing functions. $S(|\mu|, F, l_1)$ is defined for a beam slope $\mu = \cot\theta$ from the surface point $F(\xi_0, \gamma_0)$ with an observation length l_1. $S(\mu_1, F_1, \infty)$ is defined for an incidence beam slope $\mu_1 = \cot\theta_1$ emanating from the surface point $F_1(\xi_1\xi_0 + \mu l_1, \gamma_1)$ with an infinite observation length.

The use of (1), (2) yields

$$S_2(\mu, \mu_1, F, F_1, l_1) = \begin{cases} \Pi_1 \dfrac{[P(\xi_0) - P(-\infty)]^{\Lambda(|\mu|)}}{[P(\xi_0 + |\mu| l_1) - P(-\infty)]^{\Lambda(|\mu|) - \Lambda(\mu_1)}} \\ \qquad \text{cases } (a_{1,2}) \text{ with} \quad \theta \in \left[-\dfrac{\pi}{2}; 0\right] \cup \left[\theta_1; \dfrac{\pi}{2}\right], \\ 0 \qquad \text{case } (a_3) \text{ with} \quad \theta \in]0; \theta_1[\end{cases} \tag{3}$$

with

$$\Pi_1 = \Upsilon(|\mu| - \gamma_0)\Upsilon(\mu_1 - \gamma_1). \tag{3a}$$

Although the sign of μ is different for cases $(a_{1,2})$ (see figure 1), the statistical shadowing function is the same. This is due to the fact that the surface slope distribution is assumed to be even, which means that the probability of obtaining negative slopes is equal to that for positive slopes.

If $l_1 = 0$, then $F_1 \equiv F$ (see figure 1), meaning that $\{\gamma_1 = \gamma_0, \mu_1 = \mu\}$ and $S_2(\mu, F, l_1) = \Upsilon(|\mu| - \gamma_0)[P(\xi_0) - P(-\infty)]^{\Lambda(|\mu|)}$, which is similar to the monostatic shadowing function with single reflection and for an infinite observation length.

The surface height and slope joint distribution with shadowing effect $p_{2\mathrm{Sh}}(\mu, \mu_1, \xi_0, \xi_1, \gamma_0, \gamma_1, l_1)$ is then expressed from the unshadowed one $p(\xi_0, \xi_1, \gamma_0, \gamma_1; l_1)$ as

$$\begin{aligned} p_{2\mathrm{Sh}}(\mu, \mu_1, \xi_0, \xi_1, \gamma_0, \gamma_1, l_1) &= p(\xi_0, \xi_1, \gamma_0, \gamma_1; l_1) S_2(\mu, \mu_1, \xi_0, \xi_1, \gamma_0, \gamma_1, l_1) \\ &\text{where} \quad \xi_1 = \xi_0 + |\mu| l_1. \end{aligned} \tag{4}$$

To illustrate (4), an uncorrelated Gaussian process with zero mean is used:

$$p(\xi_0, \xi_1, \gamma_0, \gamma_1; l_1) = \frac{1}{(2\pi\omega\sigma)^2} \exp\left(-\frac{\xi_0^2}{2\omega^2} - \frac{\xi_1^2}{2\omega^2} - \frac{\gamma_0^2}{2\sigma^2} - \frac{\gamma_1^2}{2\sigma^2}\right), \tag{5}$$

where $\{\omega^2, \sigma^2\}$ are the surface height and slope variances, respectively. We can note that the above equation is independent of l_1 since the correlation is omitted.

Use of the variable transformations

$$\begin{aligned} h_0 &= \xi_0/(\omega\sqrt{2}) \qquad \zeta_0 = \gamma_0/(\sigma\sqrt{2}) \\ h_1 &= \xi_1/(\omega\sqrt{2}) \qquad \zeta_1 = \gamma_1/(\sigma\sqrt{2}) \end{aligned} \qquad y_1 = l_1/L_c, \tag{6}$$

and

$$\begin{aligned} &p(\xi) = \frac{1}{\omega\sqrt{2\pi}}\exp\left(-\frac{\xi^2}{2\omega^2}\right) \Rightarrow P(\xi) = \frac{1}{2}\mathrm{erf}\left(\frac{\xi}{\omega\sqrt{2}}\right), \\ &\mathrm{d}\xi_0\,\mathrm{d}\xi_1\,\mathrm{d}\gamma_0\,\mathrm{d}\gamma_1 = 2(\omega\sigma)^2\,\mathrm{d}h_0\,\mathrm{d}h_1\,\mathrm{d}\zeta_0\,\mathrm{d}\zeta_1 \end{aligned} \tag{7}$$

leads for the $(a_{1,2})$ cases, with $\nu \in [-\nu_1; \infty[$ to

$$\begin{aligned} P_{2\mathrm{Sh}} = {} & [\Upsilon(\nu - \zeta_0)\exp(-\zeta_0^2)/\sqrt{\pi}] \times [\Upsilon(\nu_1 - \zeta_1)\exp(-\zeta_1^2)/\sqrt{\pi}] \\ & \times [\{1 - \mathrm{erfc}(h_0)/2\}^{\Lambda(|\nu|)}\exp(-h_0^2)/\sqrt{\pi} \\ & \times \{1 - \mathrm{erfc}(h_0 + y_1|\nu|\eta)/2\}^{\Lambda(\nu_1)-\Lambda(|\nu|)}\exp\{-(h_0 + y_1|\nu|\eta)^2\}/\sqrt{\pi}], \end{aligned} \tag{8}$$

with

$$\begin{aligned} &\Lambda(\nu) = [\exp(-\nu^2) - \nu\sqrt{\pi}\,\mathrm{erfc}(\nu)]/(2\nu\sqrt{\pi}) \\ &\nu_1 = \mu_1/(\sigma\sqrt{2}) \qquad \nu = \mu/(\sigma\sqrt{2}) \\ &\eta = \sigma L_c/\omega \end{aligned} \tag{8a}$$

where erf is the error function, $\mathrm{erfc}(x) = 1 - \mathrm{erf}(x)$ and L_c denotes the surface correlation length. For a Gaussian surface height autocorrelation function, we obtain $\eta = \sqrt{2}$.

In (8), since $|\nu| \in [\nu_1; \infty[$ we obtain $\Lambda(\nu_1) \geqslant \Lambda(\nu) \geqslant 0 \Rightarrow \Lambda(\nu_1) - \Lambda(\nu) \geqslant 0$, involving $[1 - \mathrm{erfc}(\cdots)/2]^{\Lambda(\nu_1)-\Lambda(|\nu|)} \in [0; 1]$ because $[1 - \mathrm{erfc}(\cdots)/2] \in [0; 1]$.

2.2. Simulations for the Gaussian process and surface correlation

The first two terms between brackets on the right-hand side of (8) denote the restriction over the surface-normalized slopes $\{\zeta_0, \zeta_1\}$, respectively. They are independent of the normalized distance y_1. In figure 2, they are represented versus $\{\zeta_0, \zeta_1\}$, for $\nu_1 = \{1, 0.5\}$. The slope distribution according to ζ_0 is not equal to zero for $\zeta_0 \leqslant \nu$, whereas that defined with respect to ζ_1 is reduced to the range $\zeta_1 \leqslant \nu_1$. Both distributions are not equal to zero if $\nu \in]-\infty; \nu_1]$.

In figure 3, the last term on the right-hand side of (8), which characterizes the shadowed surface height distribution, is plotted versus the normalized height h_0 for $\nu_1 = \{1, 0.5\}$ and $y_1 = \{0.1, 0.5, 2\}$. Unlike the slope distributions (figure 2), we see that when y_1 decreases the slope distribution quickly increases, tending to that defined with one reflection. The amplitude of the height distribution decreases when ν_1 decreases, corresponding to grazing incidence angles or a rougher surface since $\nu_1 = \cot\theta_1/(\sigma\sqrt{2})$.

The average statistical shadowing function over the surface heights ξ_0 and slopes $\{\gamma_0, \gamma_1\}$ is expressed with $\xi_1 = \xi_0 + |\mu|l_1$ as

$$\begin{aligned} S_2(\mu, \mu_1, l_1) &= \iiint p_{2\mathrm{Sh}}(\mu, \mu_1, \xi_0, \xi_1, \gamma_0, \gamma_1, l_1)\,\mathrm{d}\xi_0\,\mathrm{d}\gamma_0\,\mathrm{d}\gamma_1 \\ &= \iiint p(\xi_0, \xi_1, \gamma_0, \gamma_1; l_1)S_2(\mu, \mu_1, \xi_0, \xi_1, \gamma_0, \gamma_1, l_1)\,\mathrm{d}\xi_0\,\mathrm{d}\gamma_0\,\mathrm{d}\gamma_1. \end{aligned} \tag{9}$$

Substituting (3) into (9), the average shadowing function is

$$S_2(\mu, \mu_1, l_1) = \begin{cases} \Lambda_1(|\mu|) \times \Lambda_1(\mu_1) \times \displaystyle\int_{-\infty}^{\infty} p(\xi_0)[P(\xi_0) - P(-\infty)]^{\Lambda(|\mu|)} \\ \quad \times p(\xi_0 + |\mu|l_1)[P(\xi_0 + |\mu|l_1) - P(-\infty)]^{\Lambda(\mu_1)-\Lambda(|\mu|)}\,\mathrm{d}\xi_0 \\ \quad \text{if} \quad \mu \in]-\infty; \mu_1] \\ 0 \qquad \text{else,} \end{cases} \tag{10}$$

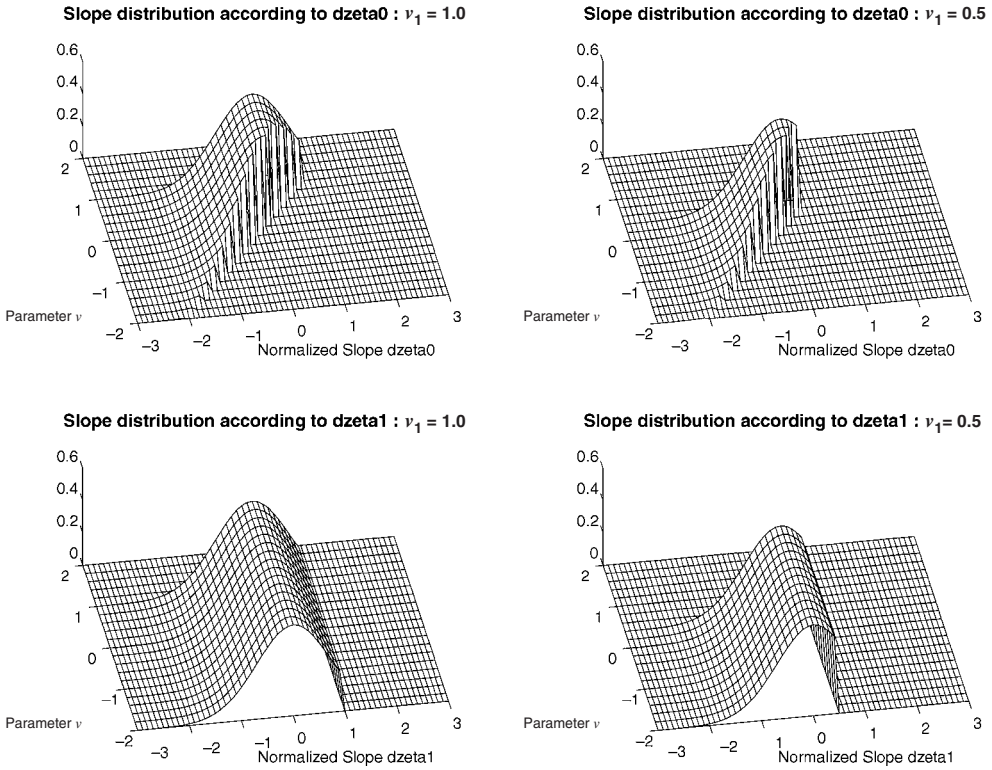

Figure 2. Top: monostatic shadowed surface slope distribution with double reflection versus the normalized slope ζ_0 for $v_1 = \{1, 0.5\}$. Bottom: that versus the normalized slope ζ_1.

with

$$\Lambda_1(x) = \int_{-\infty}^{x} p(\gamma)\,\mathrm{d}\gamma. \tag{10a}$$

The use of variable transformations (6) and (8*a*) yields for an uncorrelated Gaussian process ($\Lambda_1(x) = [1 + \mathrm{erf}(x)]/2$)

$$S_2(v, v_1, y_1) = \begin{cases} \dfrac{1}{4\pi}[1 + \mathrm{erf}(|v|)][1 + \mathrm{erf}\,(v_1)] \displaystyle\int_{-\infty}^{\infty} \exp[-h_0^2 - (h_0 + y_1|v|\eta)^2] \\ \quad \times\big[1 - \frac{1}{2}\mathrm{erfc}(h_0)\big]^{\Lambda(|v|)}[1 - \frac{1}{2}\mathrm{erfc}(h_0 + y_1|v|\eta)]^{\Lambda(v_1)-\Lambda(|v|)}\,\mathrm{d}h_0 \\ \quad \text{if} \quad v \in]-\infty; v_1] \\ 0 \qquad \text{else.} \end{cases} \tag{11}$$

In figure 4, the above equation is plotted versus $\{v, y_1\}$ for $v_1 = \{2, 1, 0.5, 0.1\}$. We can see that when the normalized distance y_1 increases, the average shadowing function decreases quickly, as $|v|$ tends to zero, corresponding to either a very rough surface or angles close to $\pm 90^\circ$. If v_1 decreases, then the amplitude of the average shadowing function decreases, and for values of $v \leqslant v_1$ it is equal to zero. This maximum value is obtained when $\{y_1 = 0, v_1 \geqslant 2\}$ ($\Lambda(2) \approx 2, 4 \times 10^{-4}$ and $\mathrm{erf}(2) \approx 0.99$), meaning that

$$S_2(v, 2, 0) \approx \frac{1 + \mathrm{erf}(|v|)}{2\pi} \int_{-\infty}^{\infty} \exp(-2h_0^2)\,\mathrm{d}h_0 = \frac{1 + \mathrm{erf}(|v|)}{2\sqrt{2\pi}} \qquad \text{if} \quad v \in]-\infty; 2]. \tag{12}$$

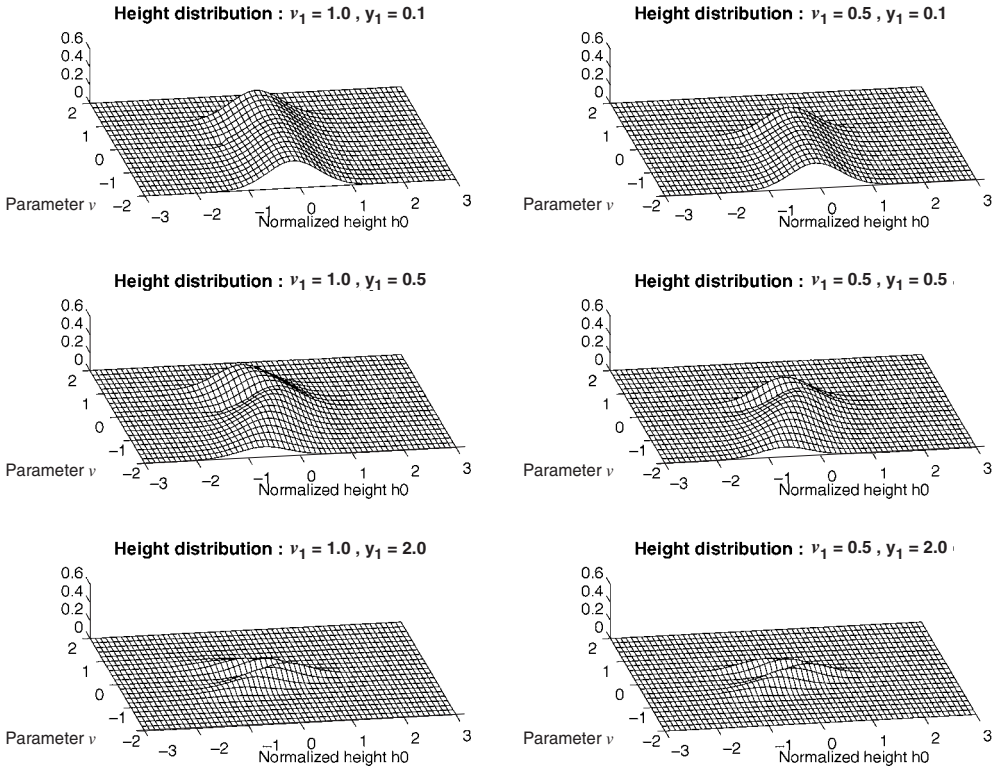

Figure 3. Monostatic shadowed surface height distribution with double reflection versus the normalized height h_0 for $y_1 = \{0.1, 0.5, 2\}$. Left: $v_1 = 1$. Right: $v_1 = 0.5$.

Now, we can calculate the integration over l_1 of the average shadowing function defined from (9) as

$$S_2(\mu, \mu_1) = \int_0^\infty S_2(\mu, \mu_1, l_1)\, \mathrm{d}l_1. \tag{13}$$

We show in the appendix, for any uncorrelated distribution, that the above equation becomes

$$S_2(v, v_1) = \begin{cases} \dfrac{\Lambda_1(|v|)\Lambda_1(v_1)}{2|\mu|[1 + \Lambda(|v|)][1 + \Lambda(v_1)/2]} & \text{if} \quad v \in]-\infty; v_1] \\ 0 & \text{else} \end{cases} \tag{14}$$

with

$$\Lambda_1(x) = \sqrt{2}\sigma \int_{-\infty}^{x} p(\gamma\sqrt{2}\sigma)\, \mathrm{d}\gamma. \tag{14a}$$

For an uncorrelated Gaussian process, Λ is given by (8a), and $\Lambda_1(v) = [1 + \mathrm{erf}(v)]/2$.

In figure 5, the $2|\mu|S_2(v, v_1)$ average monostatic shadowing function integrated over l_1 is plotted versus v for $v_1 = \{2, 1, 0.5, 0.1\}$ with an uncorrelated Gaussian process. For a very rough surface (high standard deviation of slopes σ, i.e. $|v_i| = |\mu_i|/\sigma\sqrt{2}$ small), the shadowing function decreases quickly. For incidence near 90°, corresponding to $|v_i| \to 0$, the surface is highly shaded ($S_2 \to 0$). In contrast, for normal incidence angles (v_1 close to 2), the whole surface is illuminated ($S_2 = 1$). The variation between these two asymptotic values is as much as σ.

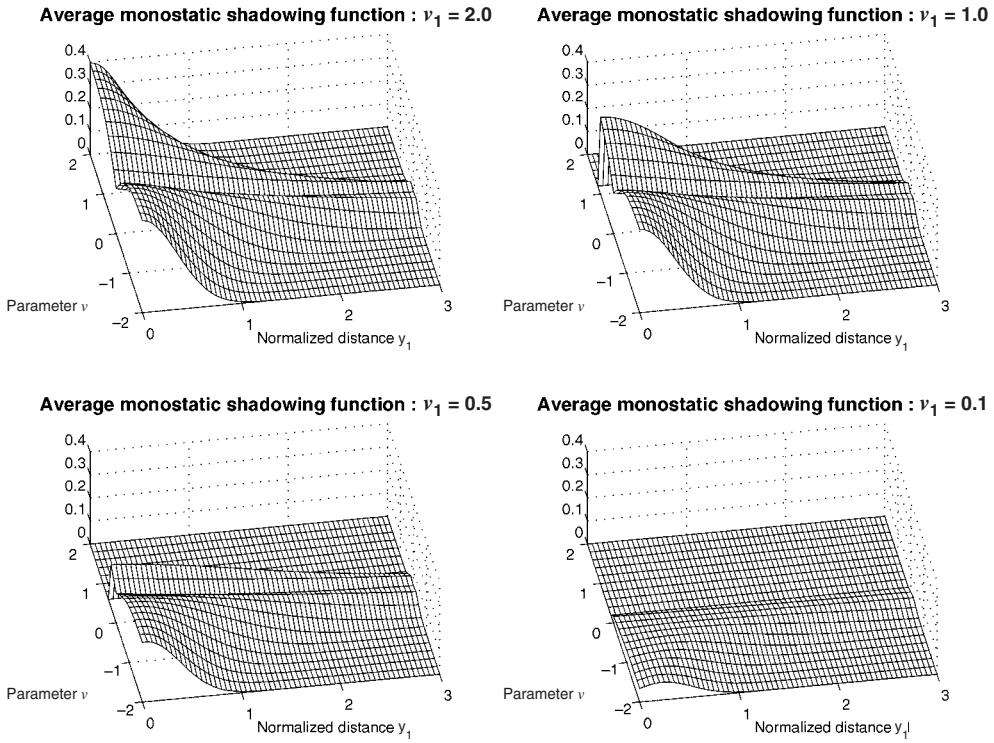

Figure 4. Average monostatic shadowing function $S_2(v, v_1, l_1)$ (equation (11)) versus $\{v, y_1\}$ for $v_1 = \{2, 1, 0.5, 0.1\}$ with an uncorrelated Gaussian process.

2.3. Monostatic statistical shadowing function with multiple reflection

In this section the monostatic statistical shadowing function with $n' = n + 1$ reflections is investigated. Only the $(a_{1,2})$ cases of figure 1 are treated since the (a_3) case is null. Therefore $\theta_p \leqslant \theta_{p-1}$ with $\theta_p \in [0; \pi/2]$ (see figure 6). We can note for $\theta_0 \in [-\pi/2; 0]$ (case (a_1)) that the shadowing effect is the same. As shown in figure 6, the monostatic statistical shadowing function with n' reflections $S_{n'}$ represents the probability that the n'-bounced waves are not intercepted by the surface. Then, we can write

$$S_{n+1}(\{\mu_n\}, \{F_n\}, \{l_n\}) = \prod_{p=0}^{p=n} S(\mu_p, F_p, l_{p+1}), \tag{15}$$

with

$$\begin{aligned} &l_{n+1} = \infty \qquad \mu_0 \to |\mu_0| \qquad F_p \equiv F_p(\xi_p, \gamma_p) \\ &\xi_p = \xi_{p-1} + \mu_{p-1} l_p \qquad \text{for} \quad p > 0 \\ &\mu_p \geqslant \mu_{p-1}. \end{aligned} \tag{15a}$$

If the relationship $\mu_p \geqslant \mu_{p-1}$ is not valid, then the statistical shadowing function is equal to zero.

For a double reflection, $n' = 2 \Rightarrow n = 1$ and (15) becomes $S(\mu_0, F_0, l_1) \times S(\mu_1, F_1, \infty)$, which is equal to the $(a_{1,2})$ cases of (1) with $\{\mu_0, F_0\} \equiv \{|\mu|, F\}$.

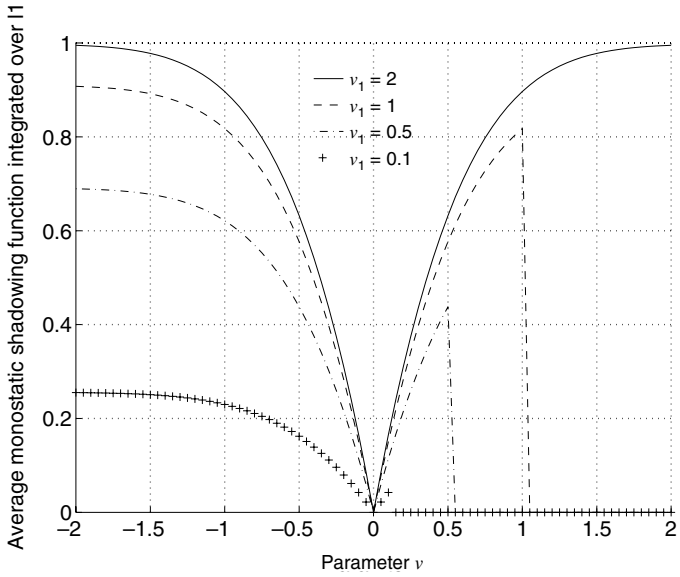

Figure 5. Average monostatic shadowing function $2|\mu|S_2(\nu, \nu_1)$ integrated over l_1 (equation (14)) versus ν for $\nu_1 = \{2, 1, 0.5, 0.1\}$ with an uncorrelated Gaussian process.

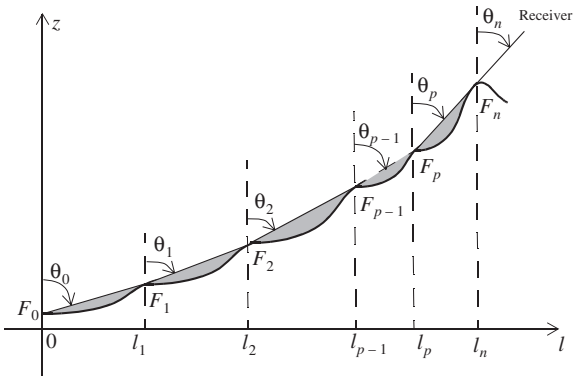

Figure 6. Illustration of the monostatic statistical shadowing function with $n' = n - 1$ reflections. This corresponds to a generalization of cases $(a_{1,2})$ of figure 1 with $\theta_p \leqslant \theta_{p-1}$ and $\theta_n \in [0; \pi/2]$.

Substituting (2) into (15), we obtain

$$S_{n+1}(\{\mu_n\}, \xi_0, \{\gamma_n\}, \{l_n\}) = \prod_{p=0}^{p=n} \Upsilon(\mu_p - \gamma_p) \left[\frac{P(\xi_p) - P(-\infty)}{P(\xi_p + \mu_p l_{p+1}) - P(-\infty)} \right]^{\Lambda(\mu_p)}, \tag{16}$$

with

$$\xi_p = \xi_0 + \sum_{m=1}^{m=p} \mu_{m-1} l_m \qquad \text{for} \quad p > 0. \tag{16a}$$

For an uncorrelated Gaussian process defined as

$$p(\{\xi_n\}, \{\gamma_n\}) = \prod_{p=0}^{p=n} p(\xi_p) \times p(\gamma_p), \tag{16b}$$

the average shadowing function integrated over ξ_0 and $\{\gamma_n\}$ is

$$S_{n+1}(\{\mu_n\},\{l_n\}) = \prod_{p=0}^{p=n} \Lambda_1(\mu_p) \int_{-\infty}^{\infty} \left[\frac{P(\xi_p) - P(-\infty)}{P(\xi_p + \mu_p l_{p+1}) - P(-\infty)} \right]^{\Lambda(\mu_p)} p(\xi_0)\,\mathrm{d}\xi_0, \tag{17}$$

with Λ_1 given by (10a).

The average shadowing function integrated over $\{l_{p+1}\}$ ($l_{n+1} = \infty$) is

$$\begin{aligned} S_{n+1}(\{\mu_n\}) = \prod_{p=0}^{p=n} \Lambda_1(\mu_p) \int_{-\infty}^{\infty} p(\xi_0)[P(\xi_0) - P(-\infty)]^{\Lambda(\mu_0)}\,\mathrm{d}\xi_0 \\ \times \left\{ \prod_{p=0}^{p=n-1} \int_{-\infty}^{\infty} [P(\xi_p + \mu_p l_{p+1}) - P(-\infty)]^{\Lambda(\mu_{p+1})-\Lambda(\mu_p)} \right. \\ \left. \times p(\xi_p + \mu_p l_{p+1})\,\mathrm{d}l_{p+1} \right\}. \end{aligned} \tag{18}$$

Using the variable transformation $\xi_{p+1} = \xi_p + \mu_p l_{p+1}$ and the appendix, we show

$$S_{n+1}(\{\nu_n\}) = \frac{\Lambda_1(\nu_0)}{1+\Lambda(\nu_0)} \prod_{p=0}^{p=n-1} \frac{\Lambda_1(\nu_{p+1})}{2\mu_p\{1 + [\Lambda(\nu_{p+1}) - \Lambda(\nu_p) + \Lambda(\nu_0)]/2\}} \qquad p > 0, \tag{19}$$

with

$$\nu_p = \mu_p/(\sigma\sqrt{2}). \tag{19a}$$

The first term on the right-hand side of (19) corresponds to the average monostatic shadowing function with single reflection for an infinite observation length. For a double reflection, $n = 1$ and (14) is found with $\{|\mu| = \mu_0, |\nu| = \nu_0\}$. Since $\mu_p \geqslant \mu_0$, from (19a) and (8a) we obtain $\nu_p \geqslant \nu_0$ and $\Lambda(\nu_p) \leqslant \Lambda(\nu_0)$, meaning that $\Lambda(\nu_0) - \Lambda(\nu_p) \geqslant 0$. This means that $S_{n+1}(\{\nu_n\}) \geqslant 0$.

To illustrate equation (19), the case where $\nu_{p+1} \approx \nu_p = \nu_0$ is considered and we obtain

$$S_{n+1}(\nu_0) = \frac{1}{(2\mu_0)^n} \frac{[\Lambda_1(\nu_0)]^{n+1}}{[1+\Lambda(\nu_0)][1+\Lambda(\nu_0)/2]^n} \geqslant S_{n+1}(\{\nu_n\}). \tag{20}$$

We can note that $S_{n+1}(\nu_0)$ is an upper bound of $(2\mu_0)^n S_{n+1}(\{\nu_n\})$.

In figure 7, for $\nu_p = \nu_0$, the monostatic average shadowing function $(2\mu_0)^n S_{n+1}(\{\nu_0\})$ integrated over $\{l_{p+1}\}$ is plotted versus the parameter ν_0 with respect to $n = n' - 1$, where n' denotes the number of reflections. We observe that the ratio of the illuminated surface to the whole surface decreases when n' increases.

3. Bistatic statistical shadowing function for any uncorrelated process

In this section, the previous model is extended to a bistatic configuration. In section 3.1, the problem is formulated for a double reflection, and section 3.2 presents simulations. In the last section, the case of multiple reflection is investigated.

3.1. Bistatic statistical shadowing function with double reflection

As shown in figures 8 and 9, the bistatic configuration is obtained from the monostatic configuration (figure 1) by adding a ray originating from an emitter with an incidence angle $\theta_i \in [-\pi/2; 0]$ defined for $l < 0$. For $l \geqslant 0$, the monostatic geometry is used with a receiver located at an incidence angle $\theta_1 \in [-\pi/2; \pi/2]$. Therefore, the bistatic statistical shadowing

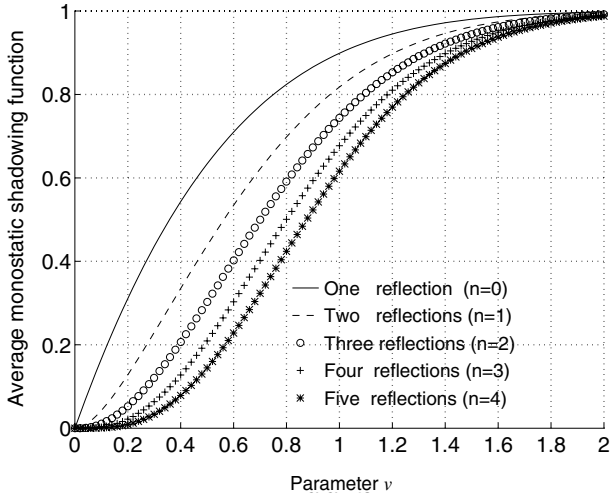

Figure 7. Average monostatic shadowing function $(2\mu_0)^n S_{n+1}(\nu_0)$ integrated over l_{p+1} (equation (20)) versus ν_0 with $\nu_p = \nu_0$ and for an uncorrelated Gaussian process.

function with double reflection S_2 represents the probability that the threefold-bounced waves denoted by the rays (i), (0), and (1) are not intercepted by the surface.

From figure 8, we can write with $\theta \in [0; \pi/2]$ that

$$S_2(\mu_i, \mu, \mu_1, F, F_1, l_1) = \begin{cases} S(|\mu_i|, F, \infty) \times S(\mu, F, l_1) \times S(\mu_1, F_1, \infty) & \text{case } (b_1) \\ S(|\mu_i|, F, \infty) \times S(\mu, F, l_1) & \text{case } (b_2) \\ 0 & \text{case } (b_3), \end{cases} \tag{21}$$

and the $\{(b_{1,2,3})\}$ cases are defined as

$$\begin{aligned} &(b_1) \text{ case} \quad \text{where} \quad \theta_1 \in [0; \pi/2] \text{ and } \theta \in [\theta_1; \pi/2] \\ &(b_2) \text{ case} \quad \text{where} \quad \theta_1 \in [-\pi/2; 0[\text{ and } \theta \in [0; \pi/2] \\ &(b_3) \text{ case} \quad \text{where} \quad \theta_1 \in [0; \pi/2] \text{ and } \theta \in]0; \theta_1[. \end{aligned} \tag{21a}$$

Case (b_1) is similar to a monostatic configuration $S(|\mu_i|, F, \infty)$ of an infinite observation length with single reflection defined according to the emitter and a monostatic configuration $S(\mu, F, l_1) \times S(\mu_1, F_1, \infty)$ with double reflection corresponding to the receiver (case (a_2) of figure 1). Case (b_2) is similar to case (a_1). Like case (a_3) of figure 1, case (b_3) is zero since the surface point F cannot be viewed by the receiver.

As shown in figure 9, with $\theta \in [-\pi/2; 0[$ we obtain

$$S_2(\mu_i, \mu, \mu_1, F, F_1, l_1) = \begin{cases} 0 & \text{case } (b_4) \\ 0 & \text{case } (b_5) \\ S(|\mu_i|, F, \infty) & \text{case } (b_6) \\ S(|\mu_i|, F, \infty) \times S(\mu_1, F, \infty) & \text{case } (b_7) \end{cases} \tag{22}$$

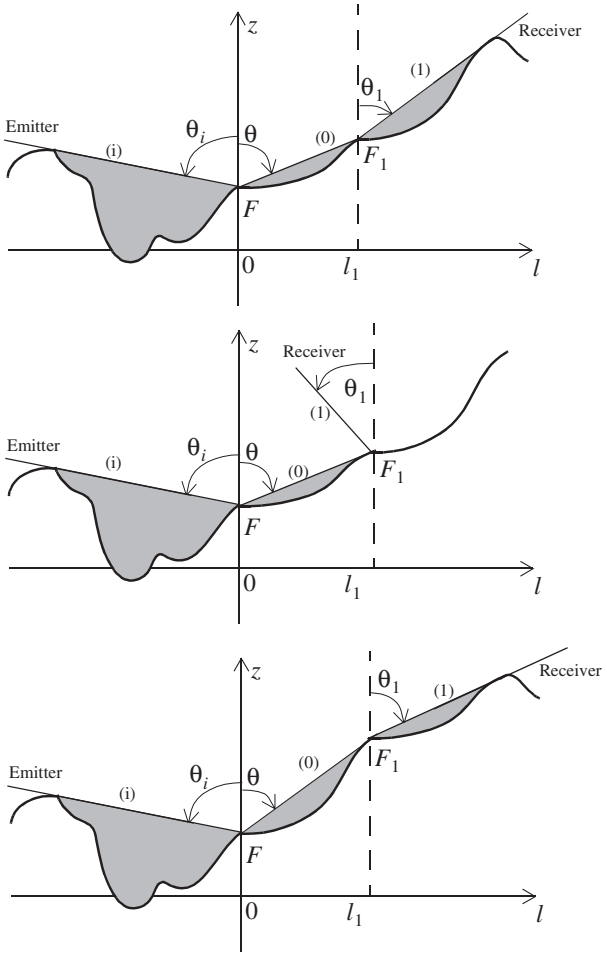

(b_1) *case where* $\begin{cases}\theta_1 \in [0;\pi/2] \\ \theta \in [\theta_1;\pi/2]\end{cases}$

(b_2) *case where* $\begin{cases}\theta_1 \in [-\pi/2;0[\\ \theta \in [0;\pi/2]\end{cases}$

(b_3) *case where* $\begin{cases}\theta_1 \in [0;\pi/2] \\ \theta \in \ ]0;\theta_1[\end{cases}$

Figure 8. Bistatic statistical shadowing function with double reflection for $\theta_i \in [-\pi/2; 0]$ and $\theta \in [0; \pi/2]$. In this case $l_1 \geqslant 0$. The surface point $F(\xi_0, \gamma_0)$ is characterized by the height ξ_0 and the slope γ_0, whereas the surface point $F_1(\xi_1, \gamma_1)$ is characterized by $\{\xi_1 = \xi_0 + l_1 \cot\theta, \gamma_1\}$.

and the ranges of the cases $\{(b_{4,5,6,7})\}$ are

$$\begin{array}{lll}\text{case } (b_4) & \text{where} & \theta \in]\theta_i; 0[\\ \text{case } (b_5) & \text{where} & \theta \in [-\pi/2; \theta_i] \text{ and } \theta_1 \in [-\pi/2; \theta[\\ \text{case } (b_6) & \text{where} & \theta \in [-\pi/2; \theta_i] \text{ and } \theta_1 \in [\theta; 0[\\ \text{case } (b_7) & \text{where} & \theta \in [-\pi/2; \theta_i] \text{ and } \theta_1 \in [0; \pi/2].\end{array} \tag{22a}$$

For case (b_4), there is no double reflection. In case (b_5), the surface point F_1 cannot be viewed by the receiver since the surface is crossed by ray (1). Case (b_6) is similar to a monostatic configuration $S(|\mu_i|, F, \infty)$ with an infinite observation length, since the probability that the surface point F_1 is hidden is equal to unity. Case (b_7) is similar to a bistatic configuration with single reflection and for an infinite observation length.

In figure 10, cases $\{(b_i)\}$ are represented in the plane (θ, θ_1) with $\theta \in [-\pi/2; \pi/2]$, $\theta_1 \in [-\pi/2; \pi/2]$ and $\theta_i \in [-\pi/2; 0]$.

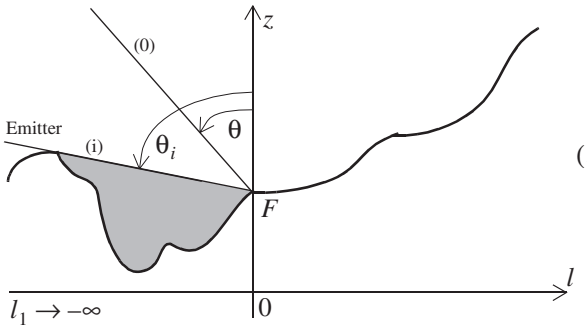

(b_4) *case where* $\begin{cases}\theta \in \ ]\theta_i;0[\\ l_1 \to -\infty\end{cases}$

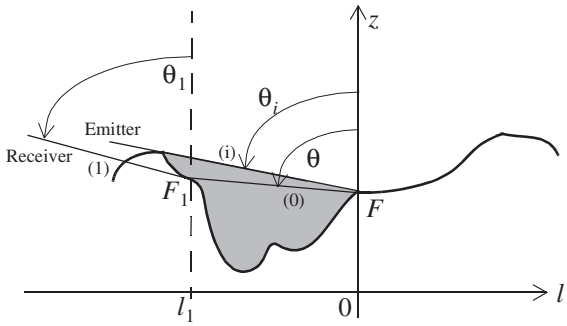

(b_5) *case where* $\begin{cases}\theta \in [-\pi/2;\theta_i] \\ \theta_1 \in [-\pi/2;\theta[\end{cases}$

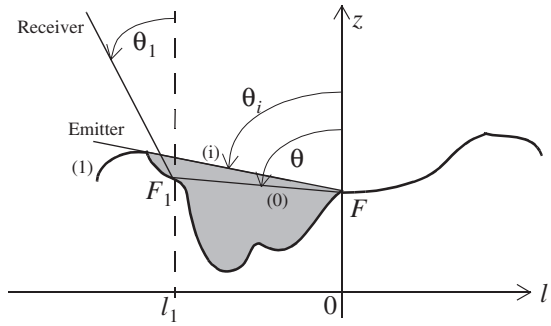

(b_6) *case where* $\begin{cases}\theta \in [-\pi/2;\theta_i] \\ \theta_1 \in [\theta;0[\end{cases}$

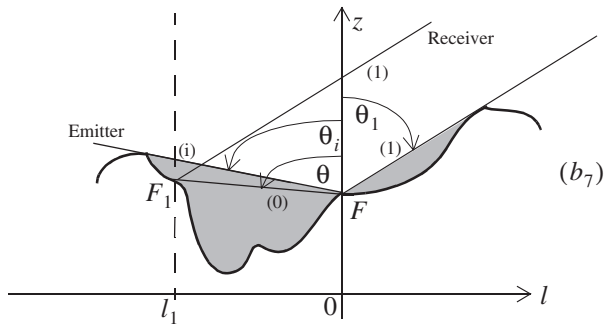

(b_7) *case where* $\begin{cases}\theta \in [-\pi/2;\theta_i] \\ \theta_1 \in [0;\pi/2]\end{cases}$

Figure 9. Bistatic statistical shadowing function with double reflection for $\theta_i \in [-\pi/2; 0]$ and $\theta \in [-\pi/2; 0[$. In this case $l_1 \leqslant 0$. The surface point $F(\xi_0, \gamma_0)$ is characterized by the height ξ_0 and the slope γ_0, whereas the surface point $F_1(\xi_1, \gamma_1)$ is characterized by $\{\xi_1 = \xi_0 + l_1 \cot\theta, \gamma_1\}$.

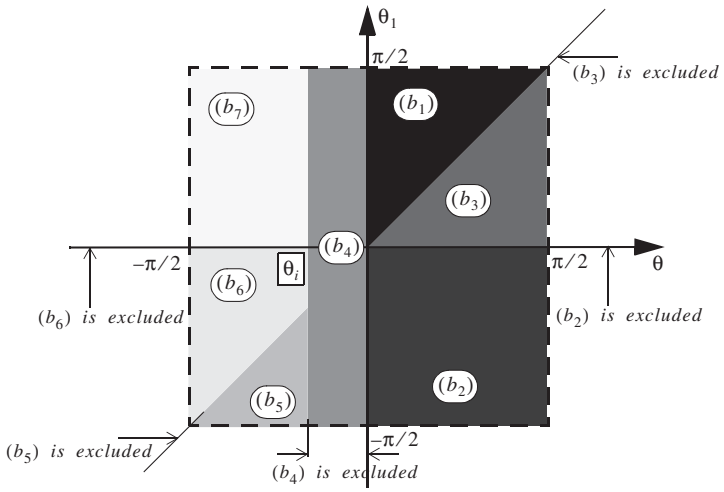

Figure 10. Representation of cases $\{(b_i)\}$ in the plane (θ, θ_1) with $\theta \in [-\pi/2; \pi/2]$, $\theta_1 \in [-\pi/2; \pi/2]$, and $\theta_i \in [-\pi/2; 0]$.

Using (2) and combining (21) with (22), we obtain

$$S_2(\mu_i, \mu, \mu_1, F, F_1, l_1) = \begin{cases} \Pi_{b_1} \times \dfrac{[P(\xi_0) - P(-\infty)]^{\Lambda(|\mu_i|)+\Lambda(\mu)}}{[P(\xi_0 + \mu l_1) - P(-\infty)]^{\Lambda(\mu)-\Lambda(\mu_1)}} & \text{case } (b_1) \\ \Pi_{b_2} \times \dfrac{[P(\xi_0) - P(-\infty)]^{\Lambda(|\mu_i|)+\Lambda(\mu)}}{[P(\xi_0 + \mu l_1) - P(-\infty)]^{\Lambda(\mu)}} & \text{case } (b_2) \\ \Upsilon(|\mu_i| - \gamma_0) \times [P(\xi_0) - P(-\infty)]^{\Lambda(|\mu_i|)} & \text{case } (b_6) \\ \Pi_{b_7} \times [P(\xi_0) - P(-\infty)]^{\Lambda(|\mu_i|)+\Lambda(\mu_1)} & \text{case } (b_7) \\ 0 & \text{cases } (b_{3,4,5}) \end{cases} \tag{23}$$

with

$$\begin{aligned} \Pi_{b_1} &= \Upsilon(|\mu_i| + \gamma_0)\Upsilon(\mu - \gamma_0)\Upsilon(\mu_1 - \gamma_1) \\ \Pi_{b_2} &= \Upsilon(|\mu_i| + \gamma_0)\Upsilon(\mu - \gamma_0) \\ \Pi_{b_7} &= \Upsilon(|\mu_i| + \gamma_0)\Upsilon(\mu_1 - \gamma_0), \end{aligned} \tag{23a}$$

and

$$\begin{array}{llll} \text{case } (b_1) & \text{where} & \mu_1 \in [0; \infty[& \mu \in [0; \mu_1] \\ \text{case } (b_2) & \text{where} & \mu_1 \in]-\infty; 0[& \mu \in [0; \infty] \\ \text{case } (b_6) & \text{where} & \mu_1 \in]-\infty; \mu] & \mu \in [\mu_i; 0] \\ \text{case } (b_7) & \text{where} & \mu_1 \in [0; \infty[& \mu \in [\mu_i; 0[\\ \text{case } (b_3) & \text{where} & \mu_1 \in [0; \infty[& \mu \in]\mu_1; \infty[\\ \text{case } (b_4) & \text{where} & & \mu \in]-\infty; \mu_i[\\ \text{case } (b_5) & \text{where} & \mu_1 \in]\mu; 0[& \mu \in [\mu_i; 0] \\ \text{with} & \{\mu_1, \mu\} \in]-\infty; \infty[& \text{and} & \mu_i \in]-\infty; 0]. \end{array} \tag{23b}$$

In (23*a*), we can notice for the $\Upsilon(|\mu_i| + \gamma_0)$ term that the sign of γ_0 is positive because the emitter is defined for $l < 0$.

Figure 11 illustrates the $\{(b_i)\}$ cases in the plane (μ, μ_1) with $\{\mu_1, \mu\} \in]-\infty; \infty[$ and $\mu_i \in]-\infty; 0]$.

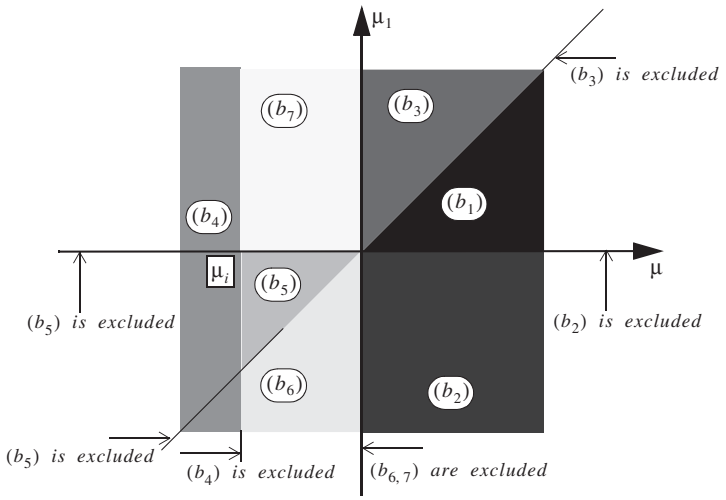

Figure 11. Representation of cases $\{(b_i)\}$ in the plane (μ, μ_1) with $\mu \in]-\infty; \infty[$, $\mu_1 \in]-\infty; \infty[$ and $\theta_i \in]-\infty; 0]$.

3.2. Discussion

For an uncorrelated Gaussian process defined as (5), substituting (23) into (4), using variable transformations (6) and (7), the surface height and slope joint distribution with shadowing effect $p_{2\mathrm{Sh}}(\mu_i, \mu, \mu_1, \xi_0, \xi_1, \gamma_0, \gamma_1, l_1)$ for each case (b_i) is

$$p_{2\mathrm{Sh}}(\nu_i, \nu, \nu_1, \xi_0, \xi_1, \gamma_0, \gamma_1, l_1) \tag{24}$$

$$= \text{case } (b_1) \begin{cases} [\Upsilon(|\nu_i| + \zeta_0)\Upsilon(\nu - \zeta_0)\exp(-\zeta_0^2)/\sqrt{\pi}] \\ \times[\Upsilon(\nu_1 - \zeta_1)\exp(-\zeta_1^2)/\sqrt{\pi}] \\ \times[\{1 - \mathrm{erfc}(h_0)/2\}^{\Lambda(|\nu_i|)+\Lambda(\nu)}\exp(-h_0^2)/\sqrt{\pi} \\ \times\{1 - \mathrm{erfc}(h_0 + y_1\nu\eta)/2\}^{\Lambda(\nu_1)-\Lambda(|\nu|)} \\ \times\exp\{-(h_0 + y_1\nu\eta)^2\}/\sqrt{\pi}] \end{cases} \tag{24a}$$

$$= \text{case } (b_2) \begin{cases} [\Upsilon(|\nu_i| + \zeta_0)\Upsilon(\nu - \zeta_0)\exp(-\zeta_0^2)/\sqrt{\pi}] \\ \times[\{1 - \mathrm{erfc}(h_0)/2\}^{\Lambda(|\nu_i|)+\Lambda(\nu)}\exp(-h_0^2)/\sqrt{\pi} \\ \times\{1 - \mathrm{erfc}(h_0 + y_1\nu\eta)/2\}^{-\Lambda(|\nu|)} \\ \times\exp\{-(h_0 + y_1\nu\eta)^2\}/\sqrt{\pi}], \end{cases} \tag{24b}$$

$$= \text{case } (b_6) \begin{cases} [\Upsilon(|\nu_i| + \zeta_0)\exp(-\zeta_0^2)/\sqrt{\pi}] \\ \times[\{1 - \mathrm{erfc}(h_0)/2\}^{\Lambda(|\nu_i|)}\exp(-h_0^2)/\sqrt{\pi}], \end{cases} \tag{24c}$$

$$= \text{case } (b_7) \begin{cases} [\Upsilon(|\nu_i| + \zeta_0)\Upsilon(\nu_1 - \zeta_0)\exp(-\zeta_0^2)/\sqrt{\pi}] \\ \times[\{1 - \mathrm{erfc}(h_0)/2\}^{\Lambda(|\nu_i|)+\Lambda(\nu_1)}\exp(-h_0^2)/\sqrt{\pi}], \end{cases} \tag{24d}$$

$$= \text{cases } (b_{3,4,5}) \quad 0, \tag{24e}$$

with

$$\nu_i = \mu_i/(\sigma\sqrt{2}) \qquad \nu_1 = \mu_1/(\sigma\sqrt{2}) \qquad \nu = \mu/(\sigma\sqrt{2}), \tag{25}$$

and in (23*b*) the ranges of cases (b_i), $\{\mu_i, \mu_1, \mu\}$ are substituted by $\{\nu_i, \nu_1, \nu\}$.

The comparison of (24*a*) with (8) shows, for the bistatic configuration, an additional restriction over the surface-normalized slopes ζ_0 represented by the $\Upsilon(|\nu_i|+\zeta_0)$ term, and over the surface-normalized heights h_0, the additional term $\{1-\mathrm{erfc}(h_0)/2\}^{\Lambda(|\nu_i|)}$. This corresponds to the contribution of the shadowing effect according to the emitter. The (b_6) case is similar to a monostatic case with an infinite observation length, which carries a restriction over the surface-normalized slopes ζ_0 and modifies the unshadowed surface height distribution. Their effect is represented in figure 2 of [16]. The (b_7) case is similar to a bistatic configuration with an infinite observation length and it is depicted in figure 13 of [16].

Substituting (23) into (9), the bistatic average shadowing function over $\{h_0, \zeta_0, \zeta_1\}$ with double reflection is expressed for any uncorrelated process as

$$S_2(\mu_i, \mu, \mu_1, l_1) \tag{26}$$

$$= \text{case } (b_1) \begin{cases} [\Lambda_1(|\nu_i|) + \Lambda_1(\nu) - 1] \times \Lambda_1(\nu_1) \times \displaystyle\int_{-\infty}^{\infty} p(\xi_0)p(\xi_0+\mu l_1) \\ \times [P(\xi_0) - P(-\infty)]^{\Lambda(|\nu_i|)+\Lambda(\nu)} \\ \times [P(\xi_0+\mu l_1) - P(-\infty)]^{\Lambda(\nu_1)-\Lambda(|\nu|)}\,\mathrm{d}\xi_0, \end{cases} \tag{26a}$$

$$= \text{case } (b_2) \begin{cases} [\Lambda_1(|\nu_i|) + \Lambda_1(\nu) - 1] \times \Lambda_1(\nu_1) \displaystyle\int_{-\infty}^{\infty} p(\xi_0)p(\xi_0+\mu l_1) \\ \times [P(\xi_0) - P(-\infty)]^{\Lambda(|\nu_i|)+\Lambda(\nu)} \\ \times [P(\xi_0+\mu l_1) - P(-\infty)]^{-\Lambda(|\nu|)}\,\mathrm{d}\xi_0, \end{cases} \tag{26b}$$

$$= \text{case } (b_6) \quad \Lambda_1(|\nu_i|) \times [1+\Lambda(|\nu_i|)]^{-1}, \tag{26c}$$

$$= \text{case } (b_7) \quad [\Lambda_1(|\nu_i|) + \Lambda_1(\nu_1) - 1] \times [1+\Lambda(|\nu_i|) + \Lambda(\nu_1)]^{-1}, \tag{26d}$$

$$= \text{cases } (b_{3,4,5}) \quad 0, \tag{26e}$$

where $\{\Lambda, \Lambda_1\}$ is defined as (2*b*) and (14*a*), respectively. For a Gaussian process it is equal to $\Lambda_1(x) = [1+\mathrm{erf}(x)]/2$ and Λ is given by (8*a*).

We can note that

$$\int_{-\infty}^{\infty} p(\zeta)\,\mathrm{d}\zeta = 1 = \int_{-\infty}^{|x_1|} p(\zeta)\,\mathrm{d}\zeta + \int_{-\infty}^{x_2} p(\zeta)\,\mathrm{d}\zeta - \int_{-|x_1|}^{x_2} p(\zeta)\,\mathrm{d}\zeta, \tag{27}$$

meaning that

$$\int_{-|x_1|}^{x_2} p(\zeta)\,\mathrm{d}\zeta = \Lambda_1(|x_1|) + \Lambda_1(x_2) - 1. \tag{28}$$

This explains in (26*a*) and (26*b*) the term $\Lambda_1(|\nu_i|)+\Lambda_1(\nu)-1$, since the integration range of ζ_0 is $[-|\nu_i|; \nu]$. In cases $(b_{2,6,7})$ (24*b*)–(24*d*), the integration over ζ_1 is not required since the shadowed process does not depend on ζ_1. Equation (26*c*) corresponds to the average monostatic shadowing function given by (18) of [16] with a Gaussian process (Smith formulation) for an infinite observation length, whereas (26*d*) represents that for a bistatic configuration ((62), first case of [16]).

Using the same method as the appendix, the integration of $S_2(\nu_i, \nu, \nu_1, l_1)$ over l_1 leads for (26*a*) and (26*b*) to

$$S_2(\nu_i, \nu, \nu_1, l_1) \tag{29}$$

$$= \text{case } (b_1) \quad \frac{[\Lambda_1(|\nu_i|) + \Lambda_1(\nu) - 1] \times \Lambda_1(\nu_1)}{2\mu[1+\Lambda(\nu)+\Lambda(|\nu_i|)]\{1+[\Lambda(\nu_1)+\Lambda(|\nu_i|)]/2\}} \tag{29a}$$

$$= \text{case } (b_2) \quad \frac{[\Lambda_1(|\nu_i|) + \Lambda_1(\nu) - 1] \times \Lambda_1(\nu_1)}{2\mu[1+\Lambda(\nu)+\Lambda(|\nu_i|)][1+\Lambda(|\nu_i|)/2]} \tag{29b}$$

with $\{\nu_i, \nu, \nu_1\}$ given by (25).

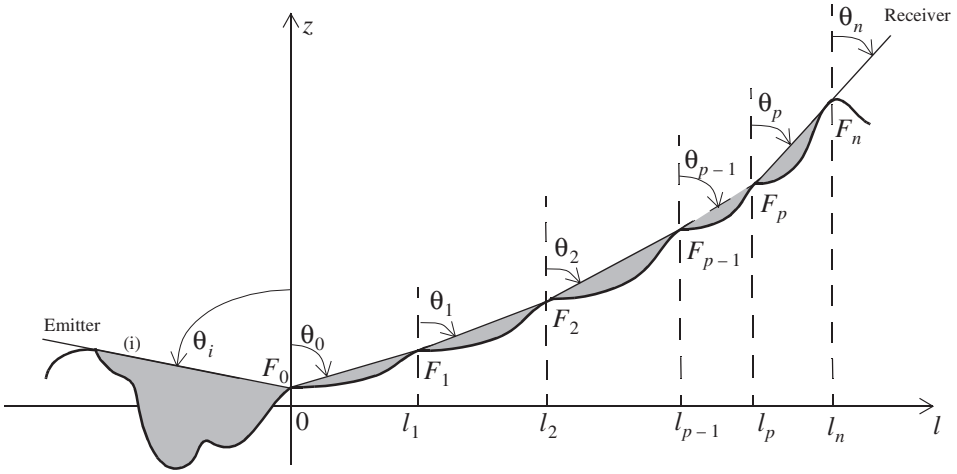

Figure 12. Illustration of the bistatic statistical shadowing function with $n' = n - 1$ reflections. $\theta_n \in [0; \pi/2]$, $\theta_i \in [-\pi/2; 0]$ and $\theta_p \leqslant \theta_{p-1}$.

If in (29*b*) $\nu_1 \to \infty$ ($\theta_1 = 0$ normal incidence), then $\Lambda(\nu_1) \to 0$ and (29*b*) is equal to (29*a*). Comparing equation (29*a*) with (14), a similar form is found, and the difference is due to the addition of the emitter. Indeed, if $|\nu_i| \to \infty$ (emitter located at normal incidence angle), then $\{\Lambda(|\nu_i|) \to 0, \Lambda_1(|\nu_i|) \to 1\}$ and the bistatic configuration is equal to the monostatic one with ν substituted by $|\nu|$.

3.3. Bistatic statistical shadowing function with multiple reflection

In this section, the bistatic statistical shadowing function with $n' = n - 1$ reflections is only depicted for case (b_1) of figure 8. This means that $\theta_n \in [0; \pi/2]$, $\theta_i \in [-\pi/2; 0]$ and $\theta_p \leqslant \theta_{p-1}$. As depicted in figure 12, $\{\theta_i, \theta_n, \theta_p\}$ denote the incidence angles of the emitter, receiver and reflections of order $p + 1$ with $p \in [0; n - 1]$. The other cases can be easily obtained by following the same method as section 3.1.

Therefore, this case is similar to a monostatic configuration with n' reflections given by (15) and a monostatic configuration with single reflection defined according to the emitter and for an infinite observation length. We obtain

$$S_{n+1}(\mu_i, \{\mu_n\}, \{F_n\}, \{l_n\}) = S(|\mu_i|, F_0, \infty) \times \prod_{p=0}^{p=n} S(\mu_p, F_p, l_{p+1}), \tag{30}$$

with the use of (15*a*).

The substitution of (2) into (30) yields

$$\begin{aligned} S_{n+1}(\mu_i, \{\mu_n\}, \{F_n\}, \{l_n\}) &= \Upsilon(|\mu_i| + \gamma_p) \times [P(\xi_0) - P(-\infty)]^{\Lambda(|\mu_i|)} \\ &\times \prod_{p=0}^{p=n} \Upsilon(\mu_p - \gamma_p) \times \left[\frac{P(\xi_p) - P(-\infty)}{P(\xi_p + \mu_p l_{p+1}) - P(-\infty)}\right]^{\Lambda(\mu_p)}. \end{aligned} \tag{31}$$

Since the emitter is defined for $l < 0$, the sign of γ_0 in $\Upsilon(|\mu_i| + \gamma_0)$ is positive. Thus, bistatic configuration (31) is obtained from the monostatic one (16) by substituting

$$\begin{aligned} &\Lambda(\mu_0) \to \Lambda(\mu_0) + \Lambda(|\mu_i|) \\ &\Upsilon(\mu_0 - \gamma_0) \to \Upsilon(\mu_0 - \gamma_0)\Upsilon(|\mu_i| + \gamma_0) \Rightarrow \gamma_0 \in [-|\mu_i|; \mu_0]. \end{aligned} \tag{31a}$$

From the results developed in section 2.3, the bistatic case can be easily studied using the above substitutions. For example, with the use of (19) and (28), the average bistatic shadowing function integrated over l_{p+1} is given by

$$S_{n+1}(\nu_i, \{\nu_n\}) = \frac{\Lambda_1(|\nu_i|) + \Lambda_1(\nu_0) - 1}{1 + \Lambda_l(\nu_0) + \Lambda_(|\nu_i|)} \times \prod_{p=0}^{p=n-1} \frac{\Lambda_1(\nu_{p+1})}{2\mu_p\{1 + [\Lambda(\nu_{p+1}) - \Lambda(\nu_p) + \Lambda(\nu_0) + \Lambda(|\nu_i|)]/2\}}. \tag{32}$$

4. Statistical shadowing function for a correlated Gaussian process

This section studies the effect of the correlation between the surface heights and slopes, assumed to be Gaussian. The statistical shadowing functions with multiple reflection developed in section 2 and given by (1), (15), (21), (22) and (30) are also valid for a correlated process. They are expressed from the monostatic statistical shadowing function $S(|\mu|, F, l_1)$ with single reflection and for a finite observation length. The assumption used arises from the derivation of this function.

Bourlier *et al* [16] studied numerically the effect of the correlation with a Gaussian process for an infinite observation length, and showed the correlation can be omitted if the parameter $\nu = \cot\theta/(\sigma\sqrt{2})$ is larger than two, where θ is the incidence angle and σ the surface slope standard deviation. This section extends the previous analysis according to the observation length, which is the additional parameter for a scattering problem with multiple scattering.

The monostatic statistical shadowing function with correlation becomes more complicated, which means the derivations of the monostatic and bistatic statistical shadowing functions with multiple reflection also become very complicated. This means, for a scattering problem with shadowing effect, the derivation of the bistatic radar cross section cannot be tractable numerically or analytically. Therefore, the aim of this section is to study the validity range when the correlation is not taken into account.

In section 4.1, for a correlated Gaussian process, the monostatic statistical shadowing function is summarized from [16]. Sections 4.2 and 4.3 compare the correlated monostatic average shadowing function with the uncorrelated one for single and double reflections, respectively.

4.1. Monostatic statistical shadowing function with single reflection

For a Gaussian process, the monostatic statistical shadowing function with correlation is expressed as ((33) of [16] for the Smith formulation denoted by the subscript S with variable transformations (6))

$$S(\nu, h_0, \zeta_0, y_1) = \begin{cases} \Upsilon(\nu - \zeta_0) \exp\left[- L_c \displaystyle\int_0^{y_t} g(\nu, h_0, \zeta_0, y)\, dy \right] & \text{if} \quad y_1 \leqslant y_t \\ \Upsilon(\nu - \zeta_0) \exp\left[- L_c \displaystyle\int_0^{y_t} g(\nu, h_0, \zeta_0, y)\, dy \right] & \\ \quad \times \left[\dfrac{1 - \operatorname{erfc}(h_0 + y_t \nu\eta)/2}{1 - \operatorname{erfc}(h_0 + y_1 \nu\eta)/2} \right]^{\Lambda(\nu)} & \text{else} \end{cases} \tag{33}$$

with $\nu = \cot\theta/(\sigma\sqrt{2})$ and $\eta = \sigma L_c/\omega$, where ω is the surface height standard deviation and L_c the surface correlation length. y_t represents the inferior limit of the observation length

where the correlation between the surface heights and slopes can be omitted. This means that the function $L_c g$ can be analytically integrated over y and gives the second term on the right-hand side of (33). For $y_1 \leqslant y_t$ the integration of the g function given in table 3 of [16] is computed numerically. It depends on the functions $\{f_{ij}(y)\}$ expressed as (28a) of [16] obtained from the normalized surface height autocorrelation function denoted as $f_0(y)$ and its derivatives $\{f_{1,2}(y)\}$ of first and second orders. For Gaussian $f_0(y) = \exp(-y^2)$ and Lorentzian $f_0(y) = 1/(1+y^2)$ normalized surface height autocorrelation functions, $\{f_{1,2}(y)\}$ are given in table 4 of [16] and $\{f_{ij}(y)\}$ are plotted in figure 4 of [16].

When the correlation is neglected we have $f_{ij} = \delta_{ij}$ (Kronecker symbol) with $\delta_{ij} = 1$ if $i = j$, else 0, and $\{y_{tG} = 3,\ y_{tL} = 4\}$ for Gaussian and Lorentzian correlations. Moreover, the exponential term $\exp[\cdots]$ of (33) is equal to

$$\left[\frac{1-\operatorname{erfc}(h_0)/2}{1-\operatorname{erfc}(h_0+y_t\nu\eta)/2}\right]^{\Lambda(\nu)}, \tag{33a}$$

and the statistical monostatic shadowing function becomes

$$S(\nu, h_0, \zeta_0, y_1) = \left[\frac{1-\operatorname{erfc}(h_0)/2}{1-\operatorname{erfc}(h_0+y_t\nu\eta)/2}\right]^{\Lambda(\nu)}. \tag{34}$$

The classical function is then found without correlation.

4.2. Average monostatic shadowing function with single reflection

To find a validity range of the monostatic statistical shadowing with single reflection and for an uncorrelated Gaussian process, the average monostatic shadowing function over $\{h_0, \zeta_0\}$ with correlation is compared with the uncorrelated one. We can note that the study of the validity domain is not made on the statistical function because this function depends on four variables (ν, h_0, ζ_0, y_1).

For a Gaussian process, the monostatic average shadowing function is

$$S(\nu, y_1) = \frac{1}{\pi}\int_{-\infty}^{\infty}\int_{-\infty}^{\infty}\exp(-h_0^2-\zeta_0^2)S(\nu, h_0, \zeta_0, y_1)\,\mathrm{d}h_0\,\mathrm{d}\zeta_0. \tag{35}$$

The cross-correlation between the surface-normalized heights h_0 and slopes ζ_0 is proportional to $f_1(0)$, where $f_1(y)$ denote the derivative of the normalized surface height autocorrelation function $f_0(y)$. Since $f_0(y)$ is even for having an Hermitian spectrum, $f_1(0) = 0$, which implies that the cross-correlation between h_0 and ζ_0 is equal to zero. In (35), this explains that $p(h_0, \zeta_0) = \exp(-h_0^2-\zeta_0^2)/\pi$.

The substitution of (33) and (34) into (35) leads, without correlation, to

$$S(\nu, y_1) = \frac{1+\operatorname{erf}(\nu)}{2\sqrt{\pi}}\int_{-\infty}^{\infty}\exp(-h_0^2)\left[\frac{1-\operatorname{erfc}(h_0)/2}{1-\operatorname{erfc}(h_0+y_1\nu\eta)/2}\right]^{\Lambda(\nu)}\mathrm{d}h_0 \tag{36}$$

without correlation,

$$S(\nu, y_1) = \begin{cases} \dfrac{1}{\pi}\displaystyle\int_{-\infty}^{\infty}\exp(-h_0^2)\,\mathrm{d}h_0\left\{\int_{-\infty}^{\nu}\exp(-\zeta_0^2)\exp[\cdots]\,\mathrm{d}\zeta_0\right\} \\ \quad \text{if} \quad y_1 \leqslant y_t \quad \text{else} \\ \dfrac{1}{\pi}\displaystyle\int_{-\infty}^{\infty}\exp(-h_0^2)\left[\frac{1-\operatorname{erfc}(h_0+y_t\nu\eta)/2}{1-\operatorname{erfc}(h_0+y_1\nu\eta)/2}\right]^{\Lambda(\nu)}\mathrm{d}h_0 \\ \quad \times\left\{\displaystyle\int_{-\infty}^{\nu}\exp(-\zeta_0^2)\exp[\cdots]\,\mathrm{d}\zeta_0\right\}. \end{cases} \tag{37}$$

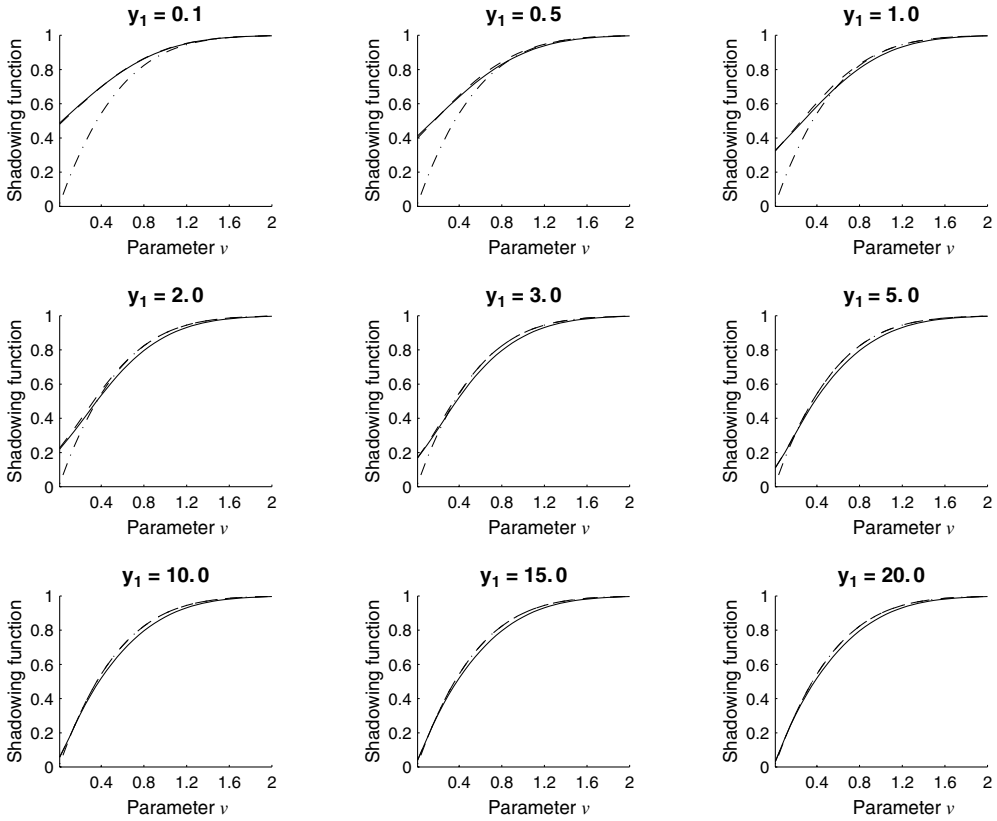

Figure 13. Average monostatic shadowing function with single reflection versus the parameter ν and the normalized observation length y_1. The full curve represents the correlated case, whereas the broken curve corresponds to the uncorrelated case. Also depicted in the chain curve are the uncorrelated results for an infinite observation length.

In figure 13, the average monostatic shadowing function with single reflection is plotted versus the parameter ν and the normalized observation length y_1. The full curve denotes the correlated case given by (37), whereas the uncorrelated case expressed from (36) is depicted with the broken curve. Also plotted in the chain curve are the uncorrelated results given by $[1+\mathrm{erf}(\nu)]/\{2[1+\Lambda(\nu)]\}$ for an infinite observation length. For small values of ν, we observe that the average monostatic shadowing function is not equal to zero and increases when y_1 decreases. If the observation length y_1 increases, the results tend to those computed for an infinite observation length. Indeed, as shown by Bourlier *et al* [22], with an absolute relative error of 0.1% the surface can be considered infinite if y_1 is larger than $\sqrt{6}/\nu$, which is similar to ν greater than $\sqrt{6}/y_1$. With $y_1 = \{1, 3, 20\}$, we obtain $\nu = \{2.45, 0.82, 0.12\}$.

In figure 14, the absolute relative difference $|S_{\mathrm{un}}(\nu, y_1) - S_{\mathrm{co}}(\nu, y_1)|/S_{\mathrm{un}}(\nu, y_1)$ between the uncorrelated $S_{\mathrm{un}}(\nu, y_1)$ and correlated $S_{\mathrm{co}}(\nu, y_1)$ average monostatic shadowing functions is plotted versus the parameter ν and the normalized observation length y_1. We can note that the maxima denoted by a cross and given for each curve in figure 14 converge toward 0.045 when y_1 increases. This means that the correlation weakly improves the results as in the case where the observation length is infinite. For ν larger than two, the average monostatic shadowing functions with and without correlation are similar, and from figure 13 the shadow

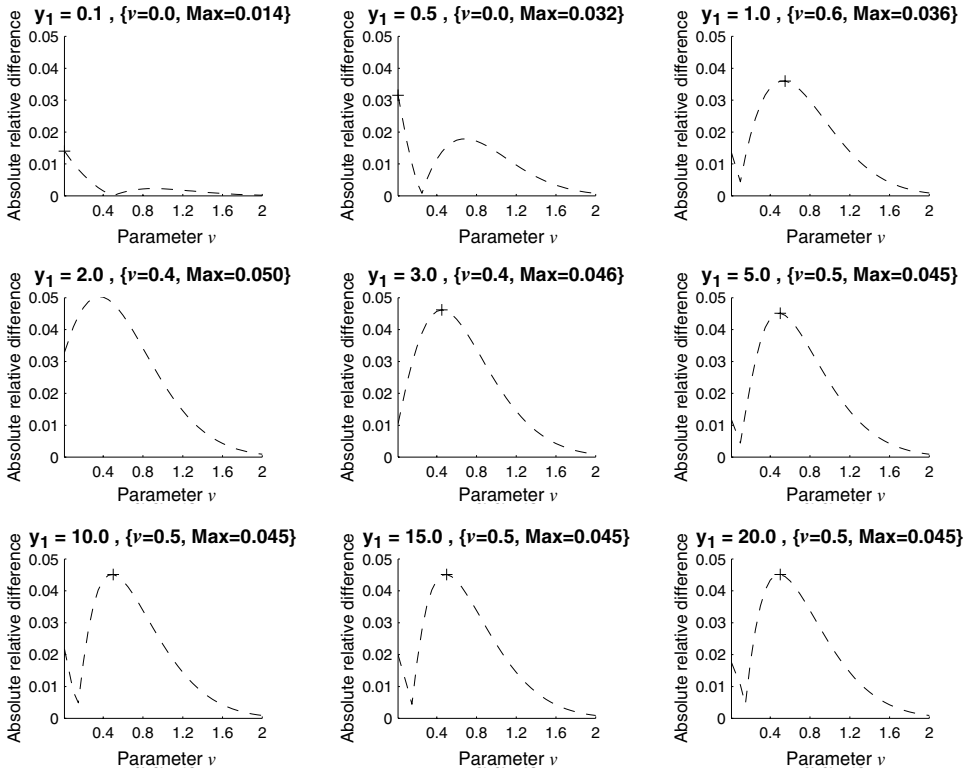

Figure 14. Absolute relative difference between the uncorrelated and correlated average monostatic shadowing functions versus the parameter ν and the normalized observation length y_1.

becomes equal to unity. Therefore, for a scattering problem, the shadow can be omitted if $\nu \geqslant 2$. Figure 16 of [16] gives versus the standard deviation of the surface slopes σ the limit incidence angle where the shadow can be neglected.

4.3. Average monostatic shadowing function with double reflection

In this section, the average monostatic shadowing function with double reflection $S_2(\mu, \mu_1, l_1)$ equal to (9) is investigated in order to study the validity range of the uncorrelated case. The statistical monostatic shadowing function with double reflection $S_2(\mu, \mu_1, F, F_1, l_1)$ is given by (1) and is valid for any correlated process. It is expressed from $S(\mu, F, l_1)$, which is given by (33) for a correlated Gaussian process with variable transformations (6).

Therefore, substituting (33) into (1) and (9), using variable transformations (6), for a correlated Gaussian process, $S_2(\nu, \nu_1, y_1)$ is written in cases $\{(a_{1,2})\}$ ($\nu \in]-\infty; \nu_1]$) as

$$S(\nu, \nu_1, y_1) = \int_{-\infty}^{\infty} G_u(\nu_1, h_1, \infty, y_t)\,\mathrm{d}h_0 \left\{ \int_{-\infty}^{|\nu|} G_c(|\nu|, h_0, \zeta_0)\,\mathrm{d}\zeta_0 \right. \tag{38}$$

$$\left. \times \left[\int_{-\infty}^{\nu_1} G_c(\nu_1, h_1, \zeta_1)\, p(h_0, h_1, \zeta_0, \zeta_1; y_1)\,\mathrm{d}\zeta_1 \right] \right\}, \qquad \text{if} \quad y_1 \leqslant y_t \tag{38a}$$

$$= \int_{-\infty}^{\infty} G_u(\nu_1, h_1, \infty, y_t) G_u(|\nu|, h_0, y_1, y_t)\,\mathrm{d}h_0 \left\{ \int_{-\infty}^{|\nu|} G_c(|\nu|, h_0, \zeta_0)\,\mathrm{d}\zeta_0 \right.$$

$$\left. \times \left[\int_{-\infty}^{\nu_1} G_c(\nu_1, h_1, \zeta_1)\, p(h_0, h_1, \zeta_0, \zeta_1; y_1)\,\mathrm{d}\zeta_1 \right] \right\}, \qquad \text{otherwise} \tag{38b}$$

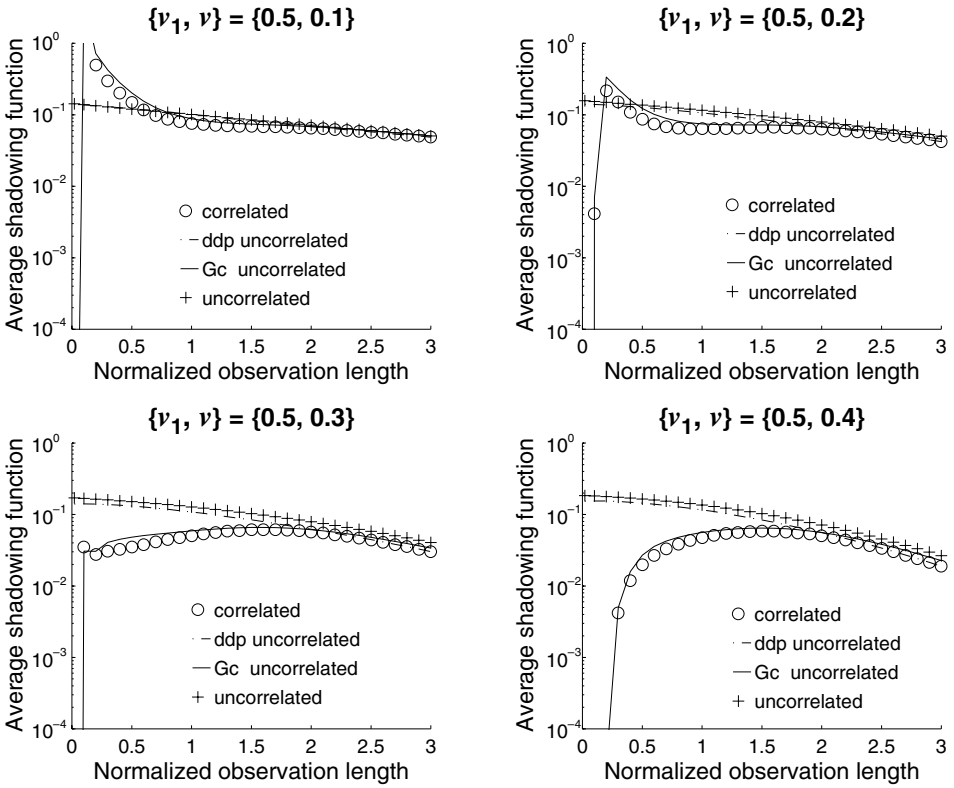

Figure 15. Average monostatic shadowing function with double reflection versus the normalized observation length y_1. Circles and crosses, the shadowing function with and without correlation, respectively. Chain curve, the case where the surface height and slope joint pdf are assumed to be uncorrelated. Full curve, the case where the correlation of the function G_c is omitted. $\nu = \{0.1, 0.2, 0.3, 0.4\}$ and $\nu_1 = 0.5$.

with

$$G_c(\nu, h_0, \zeta_0) = \exp\left[- L_c \int_0^{y_t} g(\nu, h_0, \zeta_0, y)\, \mathrm{d}y \right] \tag{38c}$$

$$G_u(\nu, h_0, y_1, y_t) = \left[\frac{1 - \mathrm{erfc}(h_0 + y_t \nu\eta)/2}{1 - \mathrm{erfc}(h_0 + y_1 \nu\eta)/2} \right]^{\Lambda(\nu)} \tag{38d}$$

$$h_1 = h_0 + y_1 |\nu| \eta. \tag{38e}$$

For the (a_3) cases $(\nu \in]\nu_1; \infty[)$, $S(\nu, \nu_1, y_1) = 0$.

We can note, for $y_1 \to \infty$, $G_u(\nu_1, h_1, \infty, y_t)$ given by (38d) is equal to $[1 - \mathrm{erfc}(h_1 + y_t \nu_1 \eta)/2]^{\Lambda(\nu_1)}$.

$p(h_0, h_1, \zeta_0, \zeta_1; y_1)$ denotes the surface height and slope joint probability density function. $p(\xi_0, \xi_1, \gamma_0, \gamma_1; l_1)$ is obtained from (21) of [16] by writing that (Bayes theorem)

$$p(\xi_0, \xi_1, \gamma_0, \gamma_1; l_1) = p(\xi, \gamma | \xi_0, \gamma_0; l_1) \times p(\xi_0, \gamma_0). \tag{38f}$$

Moreover, using variable transformations (6), in (21) of [16] $\{\{C_{ij}\}, \xi_0, \xi_1, \gamma_0, \gamma_1, l_1\}$ are substituted by $\{\{f_{ij}\}, h_0, h_1, \zeta_0, \zeta_1, y_1\}$ with the Jacobian equal to $(2\omega\sigma)^2$, and we obtain

$$p(h_0, h_1, \zeta_0, \zeta_1; y_1) = \frac{1}{\pi^2 \sqrt{f_M}} \exp[\{-f_{11}(h_0^2 + h_1^2) + f_{33}(\zeta_0^2 + \zeta_1^2) + 2 f_{12} h_0 h_1 + 2 f_{34} \zeta_0 \zeta_1 + 2 f_{13}(h_0 \zeta_0 - h_1 \zeta_1) + 2 f_{14}(h_0 \zeta_1 - h_1 \zeta_0)\}(f_M)^{-1}]. \tag{39}$$

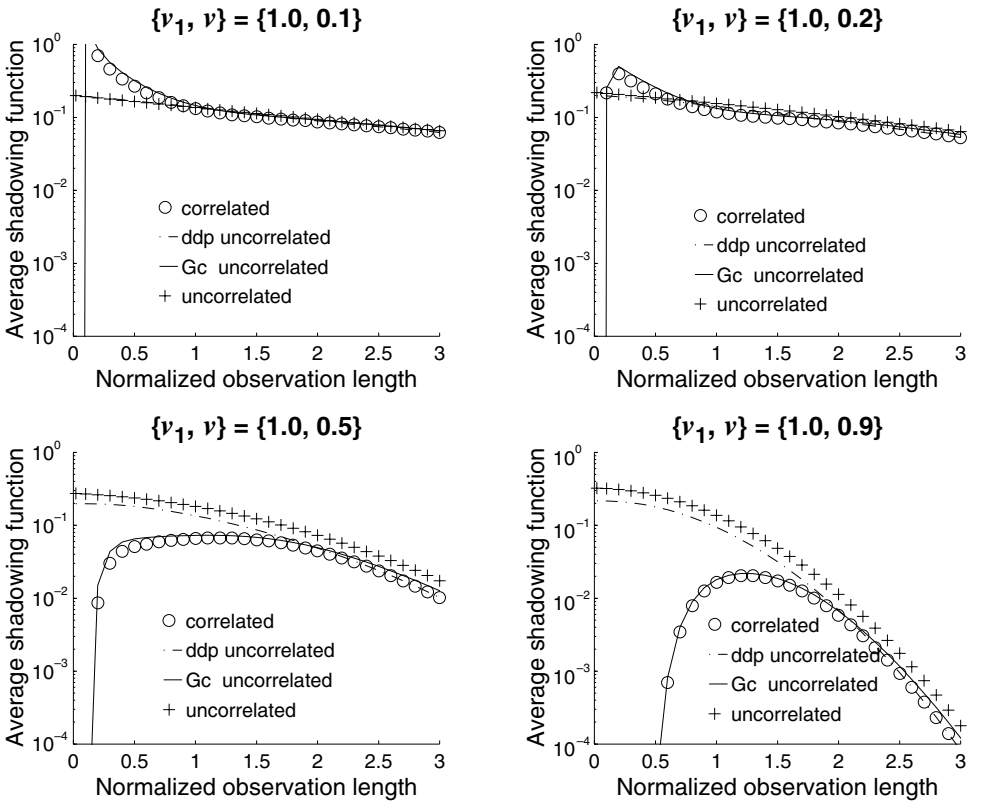

Figure 16. Average monostatic shadowing function with double reflection versus the normalized observation length y_1. Circles and crosses, the shadowing function with and without correlation, respectively. Chain curve, the case where the surface height and slope joint pdf are assumed to be uncorrelated. Full curve, the case where the correlation of the function G_c is omitted. $v = \{0.1, 0.2, 0.5, 0.9\}$ and $v_1 = 1$.

$\{f_{ij}(y_1)\}$, which depend on y_1, are given by (28a) of [16] performed from the normalized surface height autocorrelation function denoted as $f_0(y)$ and its derivatives $\{f_{1,2}(y)\}$ of first and second orders.

Equation (38) shows that the correlation increases the complexity of the model, and the average monostatic shadowing function requires threefold integrations over $\{h_0, \zeta_0, \zeta_1\}$.

When the correlation is omitted, $f_{ij} = \delta_{ij}$ (Kronecker symbol), and (39) is equal to (5) with variable transformations (6) and the Jacobian equal to $(2\omega\sigma)^2$. Moreover, (38c) becomes (33a), meaning that integrand (38b) is

$$\left[\frac{1-\operatorname{erfc}(h_0)/2}{1-\operatorname{erfc}(h_0+y_1|\nu|\eta)/2}\right]^{\Lambda(|\nu|)}[1-\operatorname{erfc}(h_1)/2]^{\Lambda(\nu_1)}\exp(-h_0^2-h_1^2-\zeta_0^2-\zeta_1^2)/\pi^2. \qquad (40)$$

Therefore, the integrations over $\{\zeta_0, \zeta_1\}$ can be performed analytically and give $\pi[1 + \operatorname{erf}(|\nu|)][1 + \operatorname{erf}(\nu_1)]/4$. Equation (11) is then found with $h_1 = h_0 + y_1|\nu|\eta$.

In figures 15–17, the average monostatic shadowing function with double reflection is plotted versus the normalized observation length y_1. The circles and crosses denote the shadowing function with (equation (38)) and without (equation (11)) correlation, respectively. The chain curve gives the case where the surface height and slope joint pdf are assumed to be uncorrelated (equation (38) where the pdf p is given by (5)). The full curve

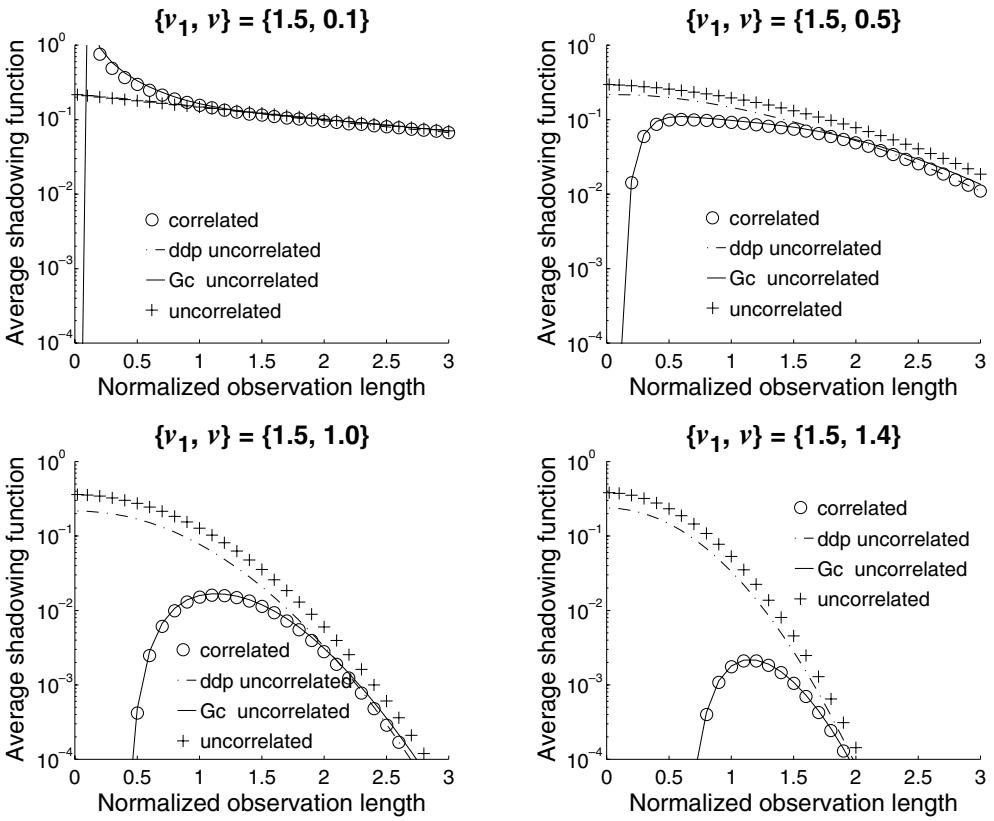

Figure 17. Average monostatic shadowing function with double reflection versus the normalized observation length y_1. Circles and crosses, the shadowing function with and without correlation, respectively. Chain curve, the case where the surface height and slope joint pdf are assumed to be uncorrelated. Full curve, the case where the correlation of the function G_c is omitted. $\nu = \{0.1, 0.5, 1, 1.4\}$ and $\nu_1 = 1.5$.

gives the case where the correlation of the function G_c is omitted (equation (38*d*) with $G_c(\nu, h_0, \zeta_0) = G_u(\nu, h_0, y_1, 0)$, which corresponds to the first term of (40), and the pdf p given by (39)). In figure 15, $\nu = \{0.1, 0.2, 0.3, 0.4\}$ and $\nu_1 = 0.5$. In figure 16, $\nu = \{0.1, 0.2, 0.5, 0.9\}$ and $\nu_1 = 1$. In figure 17, $\nu = \{0.1, 0.5, 1, 1.4\}$ and $\nu_1 = 1.5$.

For small values of the normalized observation length y_1, we observe that the difference between the correlated (circles) and uncorrelated (crosses) results is large, and decreases when y_1 increases since the correlation becomes smaller as ν_1 decreases. The comparison of the full curve (the case where the pdf is correlated with G_c uncorrelated) with the chain curve (the case where the pdf is uncorrelated with G_c correlated) shows that this discrepancy arises from the fact that the correlation on the pdf is not taken into account. Indeed, when the correlation on the pdf is not ignored with G_c uncorrelated, there is a good fit with the correlated results. We also note that the shadowing function calculated with the correlated pdf converges to zero when y_1 is close to zero since the correlated pdf is equal to zero for $y_1 = 0$, unlike the uncorrelated one.

In conclusion, as in the previous section, the uncorrelated monostatic statistical shadowing function with double reflection can be used, but for the average shadowing function the correlation between the surface heights and slopes of the joint probability density function has to be taken into account.

Since the bistatic statistical shadowing function with double reflection is expressed from the monostatic one, we obtain a similar conclusion.

5. Conclusion and discussion

In this paper, the statistical shadowing function with double and multiple reflections from a one-dimensional stationary random rough surface is investigated for monostatic and bistatic configurations. It is obtained from the monostatic statistical shadowing function with single reflection for a given observation length.

For any uncorrelated process, the statistical shadowing function is expressed from the primitive of the surface height distribution and the unit step function over the surface slopes. As in the single-reflection case, both conditions modify the height distribution and carry a restriction over the surface slopes. For an uncorrelated Gaussian process, the average shadowing function over the surface heights and slopes is performed, and the integration over the observation length of the average shadowing function is also presented. We can note that this determination is analytic and valid for any uncorrelated process.

To quantify the correlated effect between the surface heights and slopes, a correlated Gaussian process is studied. The simulations show that the correlation over the statistical shadowing function can be omitted, but for the computation of the average shadowing function the correlation has to be taken into account of the surface height and slope joint probability density function. This result allows us to have a simple statistical shadowing function.

For a scattering problem with single reflection, Bourlier *et al* [16] explain how the shadowing function effect can be introduced, and treat in [14, 15] the first-order Kirchhoff formulation. The effect of double scattering may be studied from either the IEM–IEMM–IEM2M [7–12] models or the work of Ishimaru *et al* [5, 6, 23] based on the first- and second-order Kirchhoff approximations. In both these approaches, the shadowing function is either omitted or accounted for by the average shadowing function (valid for the geometric optics approximation) with single reflection. The prospect of this paper is to include the statistical shadowing function with double reflection in the previous scattering models.

Acknowledgments

The authors would like to thank the reviewers of the paper for their relevant comments.

Appendix. Derivation of the average statistical monostatic shadowing function

This appendix presents the derivation $S_2(\mu, \mu_1)$ of the integration over l_1 of the average monostatic shadowing function $S_2(\mu, \mu_1, l_1)$ defined from (13) for any uncorrelated process.

Substituting (13) into (9), and using the variable transformation $\xi_1 = \xi_0 + |\mu| l_1$ with (3), we obtain

$$S_2(\mu, \mu_1) = \Lambda_1(|\mu|)\Lambda_1(\mu_1)\frac{1}{|\mu|}\int_{-\infty}^{\infty} p(\xi_0)[P(\xi_0) - P(-\infty)]^{\Lambda(|\mu|)}\mathrm{d}\xi_0 \times\left[\int_{\xi_0}^{\infty} p(\xi_1)[P(\xi_1) - P(-\infty)]^{\Lambda(\mu_1)-\Lambda(|\mu|)}\mathrm{d}\xi_1\right] \quad \text{if} \quad \mu \in]-\infty; \mu_1] = 0 \quad \text{else} \tag{A.1}$$

with Λ_1 given by (10*a*). The integration over ξ_1 leads for $\mu \in]-\infty; \mu_1]$ to

$$S_2(\mu,\mu_1)=\frac{\Lambda_1(|\mu|)\Lambda_1(\mu_1)}{|\mu|[1+\Lambda(\mu_1)-\Lambda(|\mu|)]}\int_{-\infty}^{\infty}p(\xi_0)[P(\xi_0)-P(-\infty)]^{\Lambda(|\mu|)}\times\{1-[P(\xi_0)-P(-\infty)]^{1+\Lambda(\mu_1)-\Lambda(|\mu|)}\}\mathrm{d}\xi_0 \tag{A.2}$$

since $P(\infty)-P(-\infty)=1$. Expanding the term over ξ_0, and integrating over ξ_0, we show

$$S_2(\mu,\mu_1)=\begin{cases}\dfrac{\Lambda_1(|\mu|)\Lambda_1(\mu_1)}{|\mu|[1+\Lambda(|\mu|)][2+\Lambda(\mu_1)]} & \text{if} \quad \mu\in\,]-\infty;\mu_1] \\ 0 & \text{else.}\end{cases} \tag{A.3}$$

References

[1] O'Donnell K A and Mendez E R 1987 Experimental study of scattering from characterized random surfaces *J. Opt. Soc. Am.* A **4** 1194–205

[2] Kim M J, Sant A J and Friberg J C 1990 Experimental study of enhanced backscattering from one- and two-dimensional surfaces *J. Opt. Soc. Am.* A **4** 569–77

[3] Johnson J T, Tsang L, Shin R T, Pak K, Chan C H, Ishimaru A and Kuga Y 1996 Backscattering enhancement of electromagnetic waves from two-dimensional perfectly conducting random rough surfaces: a comparison of Monte Carlo simulations with experimental data *IEEE Trans. Antennas Propag.* **11** 748–56

[4] Thorsos E I and Jackson D R 1991 Studies of scattering theory using numerical methods *Waves Random Media* **3** S165–90

[5] Ishimaru A, Chen J S, Phu P and Yoshitomi K 1991 Numerical, analytical, and experimental studies of scattering from very rough surfaces and backscattering enhancement *Waves Random Media* **1** S91–107

[6] Ishimaru A and Chen J S 1991 Scattering from very rough metallic and dielectric surfaces: a theory based on the modified Kirchhoff approximation *Waves Random Media* **1** 21–34

[7] Fung A K 1994 *Microwave Scattering and Emission Models and Their Applications* (Boston, MA: Artech House)

[8] Hsieh G Y, Fung A K, Nesti G, Sieber A J and Coppo P 1997 A further study of the IEM surface scattering model *IEEE Trans. Geosci. Remote Sens.* **35** 901–9

[9] Hsieh C Y 2000 Effects of bistatic multiple surface scattering from perfectly conducting surface *Electromagnetics* **20** 99–124

[10] Hsieh C Y 2000 Prediction of IEM model for backscattering enhancement *Electromagnetics* **20** 205–31

[11] Chen K S, Wu T-D, Tsay M K and Fung A K 2000 A note on the multiple scattering in an IEM model *IEEE Trans. Geosci. Remote Sens.* **38** 249–56

[12] Alavarez-Pérez J L 2000 An extension of the IEM/IEMM surface scattering model *Waves Random Media* **11** 307–29

[13] Sancer M I 1969 Shadow-corrected electromagnetic scattering from a randomly rough surface *IEEE Trans. Antennas Propag.* **17** 577–85

[14] Bourlier C, Berginc G and Saillard J 2001 Bistatic scattering coefficient from one- and two-dimensional random surfaces using the stationary phase and scalar approximation with shadowing effect—comparisons with experiments and application to the sea surface *Waves Random Media* **2** 91–118

[15] Bourlier C, Berginc G and Saillard J 2001 Theoretical study of the Kirchhoff integral from two-dimensional randomly rough surface with shadowing effect—application on the backscattering coefficient for a perfectly conducting surface *Waves Random Media* **2** 119–47

[16] Bourlier C, Berginc G and Saillard J 2001 Monostatic and bistatic statistical shadowing functions from a one-dimensional random rough surface according to the observation length: I. Single scattering *Waves Random Media* **12** 145–73

[17] Bourlier C, Saillard J and Berginc G 2000 The shadowing function *PIER (Prog. Electromagn. Res., EMW)* ed J A Kong **27** 226–87

[18] Bourlier C, Saillard J and Berginc G 2000 Effect of correlation between shadowing and shadowed points on the Wagner and Smith monostatic one-dimensional shadowing functions *IEEE Trans. Antennas Propag.* **48** 437–46

[19] Wagner R J 1966 Shadowing of randomly rough surfaces *J. Opt. Soc. Am.* **41** 138–47

[20] Smith B G 1967 Lunar surface roughness, shadowing and thermal emission *J. Geophys. Res.* **72** 4059–67

[21] Smith B G 1967 Geometrical shadowing of a random rough surface *IEEE Trans. Antennas Propag.* **15** 668–71

[22] Bourlier C, Saillard J and Berginc G 2000 Effect of the observation length on the two-dimensional shadowing function of the sea surface: application on infrared 3–13 μm emissivity *Appl. Opt.* **39** 3433–42

[23] Ishimaru A, Le C, Kuga Y, Sengers L A and Chan T K 1996 Polarimetric scattering theory for high slope rough surfaces *PIER (Prog. Electromagn. Res., EMW)* **14** 1–36